

Chapter 2

Magneto-Hydrodynamics and Operational Limits

Valentin Igochine

Abstract The main aim of the fusion research is to confine the plasma long enough for fusion power production. The required temperatures are so high that no material can tolerate direct contact. The magnetic field acts on the plasma and gives opportunity for isolation of the burning region from the surrounding materials. Different magnetic systems have different limits for plasma confinement and the plasma is lost if these limits are crossed. Thus, understanding of these limits is of primary importance for stable plasma operation. The present chapter provides a review of density, current and beta limits with particular focus on magneto-hydrodynamic instabilities in tokamaks.

2.1 Introduction to the Main Concepts of Magnetic Confinement

The main goal of fusion research is to achieve a favorable power balance in a fusion reactor, which implies the fusion power to be much higher than the input power. In order to reach this goal, the plasma has to be confined for a sufficiently long time with sufficient heat isolation at high temperatures. Assuming Deuterium-Tritium reaction, the triple product of plasma density $n[m^{-3}]$, confinement time $\tau[s]$ and plasma temperature $T[keV]$ ¹ should be sufficiently high to maintain the plasma heating solely by products of the reaction: the ignition condition is $nT\tau > 3 \times 10^{21} m^{-3} keVs$ [1]. This number is valid for the most energetically favorable reaction, between deuterium and tritium. Even in this case, the optimal reaction

¹ In plasma physics, the temperature is often given in units of the thermal energy: $T[eV] = k_B T[K]$, where Boltzmann constant $k_B = 8.6173 \times 10^{-5} [eV/K]$.

V. Igochine (✉)

Max Planck Institute for Plasma Physics, Boltzmannstr 2, 85748 Garching, Germany
e-mail: valentin.igochine@ipp.mpg.de

temperature, $T \approx 20 \text{ keV}$ ($T \approx 230 \times 10^6 \text{ K}$), is too high to be tolerated by any materials and a magnetic field is the only way to confine the plasma in a reactor under stationary conditions and isolate the burning region from the surrounding materials.

One has to start from the properties of the magnetic field to get an idea about plasma confinement. The primary action of the magnetic field on the plasma can be easily understood from single particle motion in a uniform magnetic field. A charged particle will gyrate in the plane perpendicular to the magnetic field (see Fig. 2.1a). This gyration constrains particle motion perpendicular to the magnetic field. The gyration frequency ($\omega_c = q_p B / m_p$) and the gyro-radius ($r_L = \frac{m_p v_\perp}{|q_p B|}$) follows directly from the single particle equation of motion in a uniform magnetic field taking into account the Lorentz force ($\vec{F}_L = q_p (\vec{v} \times \vec{B})$) acting on the particle (here m_p is the particle mass, q_p is the particle charge, v_\perp is the perpendicular component of the particle velocity with respect to the magnetic field \vec{B}). The important consequence of this behavior is unconstrained motion along the magnetic field. The combined perpendicular and parallel motion of the charged particle corresponds to a helical trajectory along a magnetic field line with the initial parallel velocity of the particle, v_\parallel . Restriction of the freedom of the particle motion along the magnetic field can be achieved in two ways:

- (i) variation of the magnetic field strength and/or electrostatic barriers along the field line,
- (ii) magnetic configurations with closed field lines.

The first approach is implemented in mirror systems, where variation of the magnetic field strength creates a magnetic bottle with higher magnetic field strength at both ends (see Fig. 2.1b). In this case, a particle with sufficient perpendicular velocity (v_\perp) will be confined in a region with minimal magnetic field. The particle is reflected from the high field region due to conversion of parallel velocity of the particle into perpendicular velocity. The physical reason for this behavior is the conservation of the flux enclosed by the particle trajectory over a gyro period. The conversion itself is described by the first adiabatic invariant which is approximately $\mu = \frac{m_p v_\perp^2(t)}{2B} = \text{const}$. Particles with small perpendicular velocities are not confined in the system. They move freely along the magnetic field lines and become lost; the loss condition is $v_\parallel > v_\perp \sqrt{(B_{\max} - B_{\min})/B_{\min}}$. This produces an unpopulated “loss cone” in the velocity space (Fig. 2.1c). Making the so called “mirror ratio” ($R_M = B_{\max}/B_{\min}$) high, one could reduce the loss cone. Unfortunately, Coulomb collisions change particle velocities and move new portions of the particles permanently into the loss cone. This produces a constant outflow of particles from the device along the magnetic field lines. Further complications come from anomalous losses of electrons and turbulent processes. Present configurations are able to reduce losses along the magnetic field lines but not at the level required for a reactor.

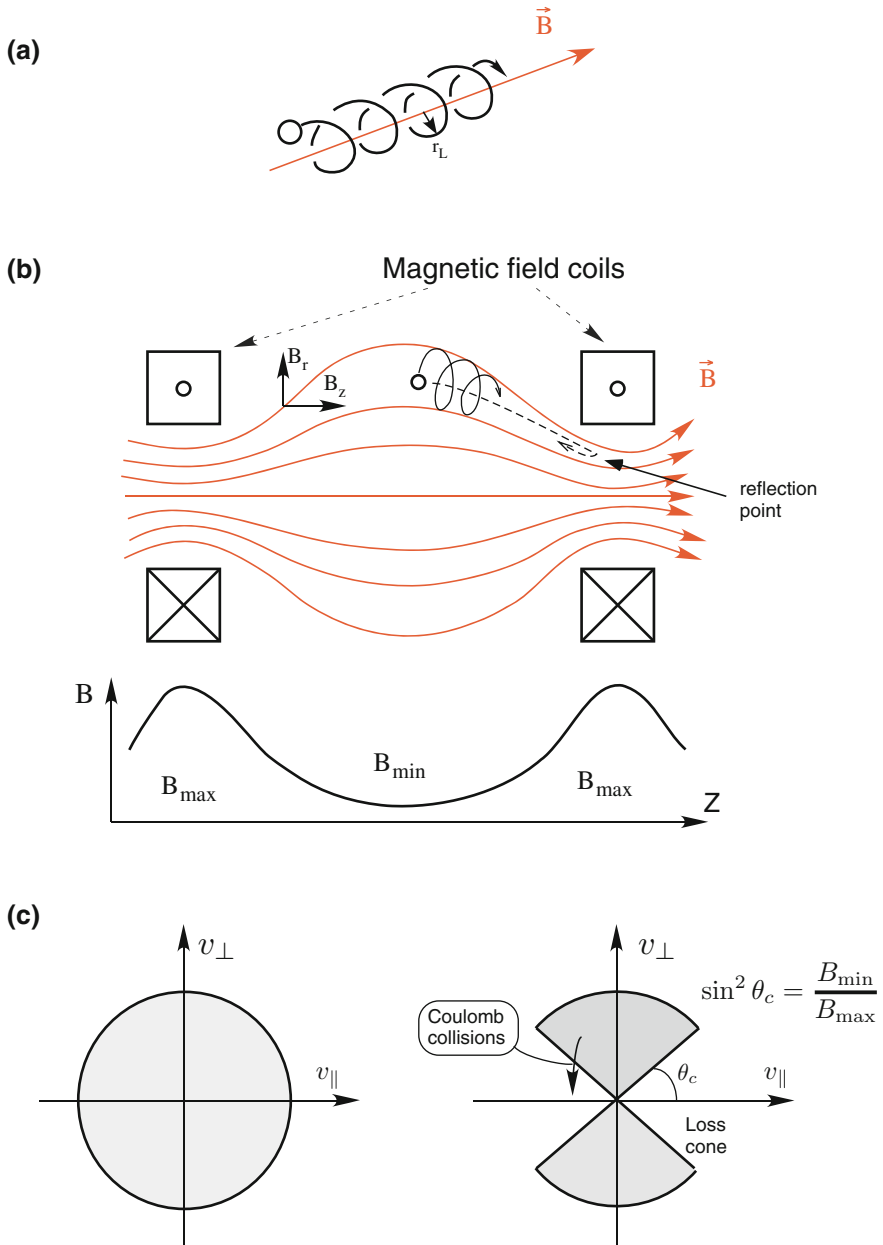


Fig. 2.1 a Single charge particle motion in a uniform magnetic field. b Magnetic bottle. Particle is reflected in high field region. c Velocity space before and after losses in the "loss cone". Collisions move new particles permanently into the loss cone

The closed field line configuration is the other approach to avoid the particle losses along the magnetic field. The simplest configuration with closed field lines can be naturally produced by bending a solenoid into a torus (Fig. 2.2a). The resulting configuration has toroidally closed magnetic field lines and solves the problem of particle losses along the magnetic field. Toroidal bending of the solenoid leads to a non-uniform magnetic field with higher values at the inner side of the torus (here the solenoid coils are close to each other) with respect to the outer side of the torus (here the distance between the coils is larger). This is why the inner part of the torus has the name “high field side” (HFS) and the other part, “low field side” (LFS). In such a configuration particle drifts becomes important.

Any force, \vec{F} , with component perpendicular to magnetic field B , results in a drift velocity ($\vec{v}_{\text{drift} \perp B} = \frac{\vec{F} \times \vec{B}}{q_p B^2}$). We use this formula to derive the main particle drifts in the toroidal configuration. Toroidal bending produces an inhomogeneous magnetic field with a gradient in the inward direction. In this case, the effective force is expressed via the magnetic moment of the particle ($\vec{F}_{\nabla B} = -\mu \nabla B$, $\mu = \frac{mv^2}{2B}$) and leads to the so-called “grad-B drift” ($\vec{v}_{\nabla B} = -\frac{m_p v_{\perp}^2}{2q_p} \frac{\nabla B \times \vec{B}}{B^3}$). The drift direction depends on the particle charge, q_p . In the configuration of Fig. 2.2a, positively charged ions drift upwards and negatively charged electrons drift downwards. The curvature of the magnetic field lines also produces a drift with effective centrifugal force ($F_c = \frac{mv_{\parallel}^2}{r}$). The curvature radius, R_c , can be expressed in terms of the magnetic field, $\frac{1}{R_c} \vec{e}_{Rc} = -\frac{\nabla B}{B}$. This drift is also charge-dependent ($\vec{v}_{Rc} = -\frac{m_p v_{\parallel}^2}{q_p} \frac{\nabla B \times \vec{B}}{B^3}$). Both drifts lead to charge separation, which produces a vertical electric field as shown in Fig. 2.2a. The resultant electric force ($\vec{F}_e = q_p \vec{E}$) produces a charge independent $\vec{E} \times \vec{B}$ drift, $\vec{v}_{E \times B} = \frac{\vec{E} \times \vec{B}}{B^2}$, which carries ions and electrons radially outward and destroys the confinement. Thus, the toroidal field alone is not sufficient for plasma confinement. The problem can be solved by the introduction of an additional poloidal field component. In this case, the field lines are helices lying on toroidally nested surfaces (see Fig. 2.2b). The additional component of the magnetic field in the poloidal direction, θ , causes the $\vec{E} \times \vec{B}$ drift to cancel, on average going in the toroidal direction, ϕ . The poloidal projection of the Pfirsch-Schlüter currents, which provide charge cancellation, is shown in Fig. 2.2b. During the last decades, this solution has shown remarkably good results and is intrinsically included in all the most successful types of fusion devices. Actually, the three most advanced magnetic confinement configurations make use of this concept: tokamaks, stellarators and reversed field pinches. The difference between these devices is in the way the poloidal field is produced, and its magnitude.

- *Tokamaks* The poloidal magnetic field is produced by the plasma current and is much smaller compared to the primary toroidal magnetic field: $B_{\theta} \ll B_{\phi}$ (see Fig. 2.2c).

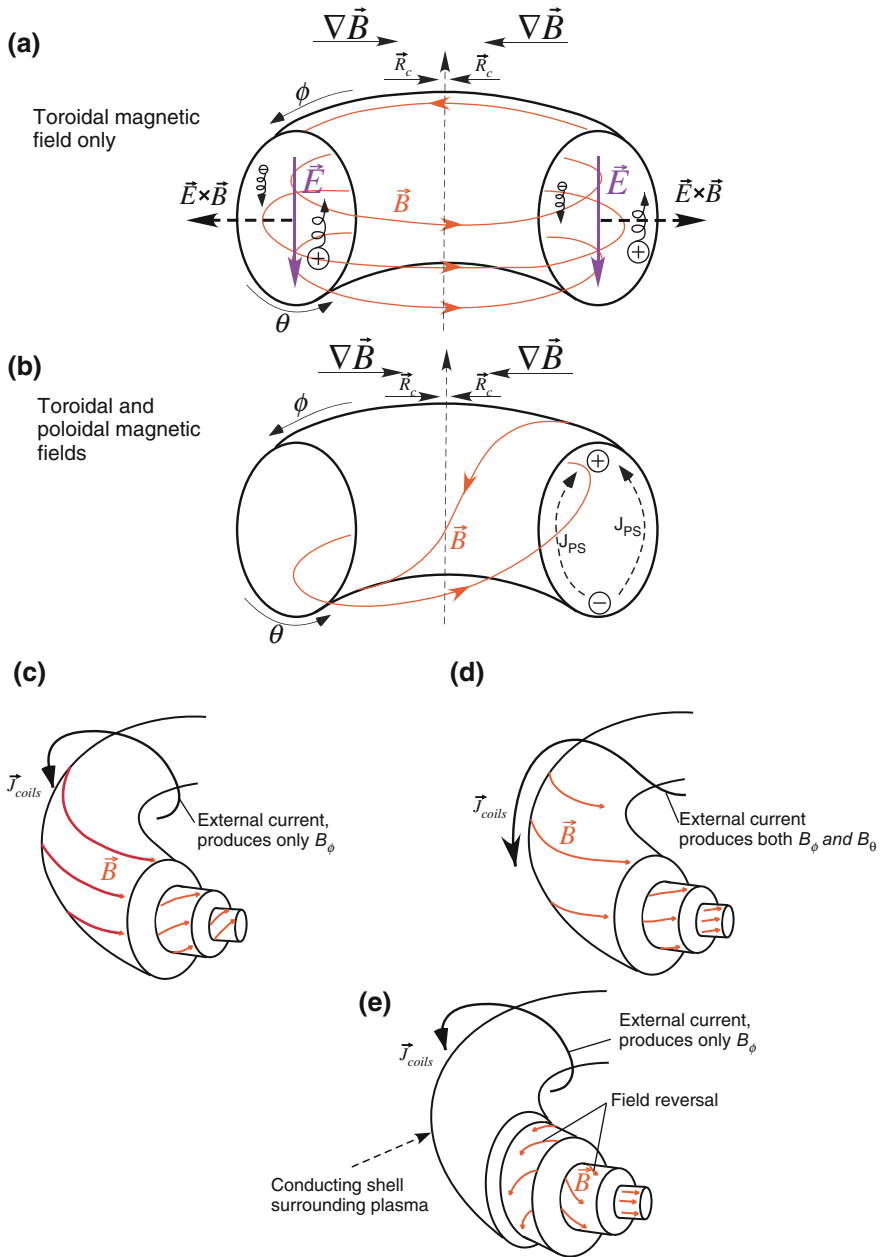


Fig. 2.2 **a** A simple toroidal magnetic field produces particle drifts, charge separation and ultimately confinement loss due to the $\vec{E} \times \vec{B}$ drift. **b** A helical magnetic field removes charge separation. **c** Tokamak. **d** Stellarator. **e** Reversed Field Pinch (RFP)

- *Stellarators* The poloidal magnetic field is produced by currents in external conductors. Thus, plasma current is not necessary for confinement (see Fig. 2.2d).
- *Reversed field pinches* The amplitude of the poloidal magnetic field produced by the plasma current is comparable with the toroidal magnetic field: $B_\theta \approx B_\phi$ (see Fig. 2.2e).

In all cases, magnetic field lines describe helices around nested toroidal surfaces, which form sequence around a single closed curve (magnetic axis). The helical winding of a field line is a topological quantity which can be characterized by the relation between the toroidal winding of the field line $\Delta\phi$ during one poloidal turn around the torus:

$$q = \frac{\Delta\phi}{2\pi} \quad (2.1)$$

This quantity, the so-called “safety factor”, is strongly linked to plasma stability, as will be shown later.

All these magnetic confinement configurations have advantages and disadvantages, which we briefly discuss here.

2.1.1 Tokamak

The word “tokamak” is an acronym of the Russian words “тороидальная камера с магнитными катушками” (toroidal’naya kamera s magnitnymi katushkami), which means “toroidal chamber with magnetic coils”. The toroidal magnetic field in the tokamak, B_ϕ , is produced by external currents in the toroidal field coils which encircle the plasma. The poloidal field, B_θ , is produced by the current in the plasma, which is induced by the transformer action where the plasma acts as the secondary transformer winding. The resulting poloidal magnetic field is much smaller than the primary toroidal magnetic field, $B_\theta \ll B_\phi$, but it has to be sustained during the whole discharge by the plasma current. In case of long-pulse or steady state operation, the current induced by the transformer is not enough. Thus alternative, non-inductive current drive schemes have to be considered for these operations, because an inductive current drive can work only temporarily. There are several different options for such non-inductive current drive in tokamaks: electron cyclotron current drive (ECCD), lower hybrid current drive (LHCD), neutral beam current drive (NBCD) and bootstrap current [2]. Among them the bootstrap current [3] is the most attractive option, which can produce a sufficiently large amount of toroidal current in big tokamaks without additional costs for the current drive system. The physical mechanism behind the bootstrap current is directly related to the inhomogeneity of the magnetic field strength which was the problem for the particle confinement in the previous section, $B \propto 1/R$. This

inhomogeneity separates particles into “trapped particles”, which are reflected by the higher magnetic field on the high field side, and “passing particles”, which are able to make a full poloidal pass along a magnetic field line. Interaction of these populations produces bootstrap current. Particle “trapping” has the same physical mechanism as discussed for the magnetic mirror above (conservation of energy plus first adiabatic invariant).

Presently, the tokamak is the most advanced concept for magnetic plasma confinement, which is the result of very intensive research during the last six decades. The temperatures required for fusion are achieved in present-day tokamaks, fusion confinement is one step away and is expected to be achieved in the next-generation experiment ITER [4] (see Fig. 2.3). In this book we will focus mainly on the tokamak device, especially on the stabilization of different instabilities in present devices and perspectives for ITER. The general overview of tokamak physics is given in J. Wesson’s comprehensive book “Tokamaks” [1]. The other configurations will be also examined in some parts of this book, insofar as this is required to understand and deal with tokamak problems.

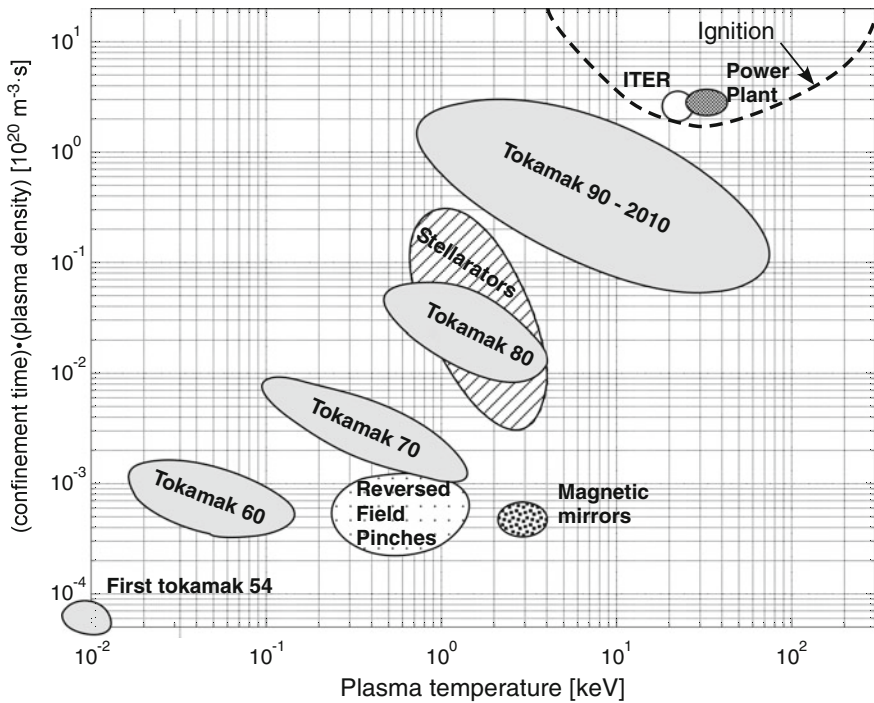


Fig. 2.3 Lawson diagram for magnetic fusion illustrates progress of the tokamaks line over several decades together with actual results from other confinement concepts (The figure is inspired by similar representation in reference [40])

2.1.2 *Stellarator*

The helical twist of the magnetic field lines can also be produced by additional external currents. In this case, plasma current is not required for confinement and the plasma operations are potentially steady-state. This is the so-called “stellarator” line of fusion research, an independent approach whose results are currently behind the tokamak line; however the concept is considered as long term solution.

The lack of plasma current avoids current-driven instabilities in stellarator. For example, there are no disruptions, no tearing modes and no resistive wall modes in stellarator. All these instabilities will be discussed in details in this book. In reality, some current is still produced by particle effects. The bootstrap current, which is an advantage for tokamaks, should be minimized by the magnetic design and/or external current drive techniques. The other line of the stellarator optimization relies on some plasma current for the confinement. The overall plasma behavior is calmer compared to the tokamak case.

The main advantages and disadvantages come from the stellarator’s complicated geometry. The concept is fully three-dimensional, in contrast to the toroidal symmetry of tokamaks. The resulting three-dimensional plasma, magnetic field, and vessel provide wide variety of different factors for optimization and at the same time make the design and optimization of the plasma confinement a very challenging task. Due to the missing toroidal symmetry, there is a branch of particle effects which can lead to confinement degradation. For example, trapped energetic particles are not necessarily confined; particle drift orbits can strongly deviate from magnetic flux surfaces around which the magnetic field lines are wound. The device must be manufactured with a high precision, because even a small misalignment of the magnetic coils changes the optimal magnetic field topology and strongly enhances these problems. The stellarator is another candidate for future fusion reactor and currently follows tokamaks in terms of triple product, $n\tau T$ (Fig. 2.3). More detailed overview of stellarator concept is given in Chap. 8 of “Fusion Physics” book [5].

2.1.3 *Reversed Field Pinch*

The main advantage of the reversed field pinch configuration is the relatively small toroidal magnetic field. The fusion reactor based on this concept could be made without superconducting coils, which are required for much stronger magnetic fields in tokamaks and stellarators but the device is intrinsically unable to have a steady state regime. Contrary to the other two concepts, RFP requires flux consumption for plasma operation and has strong pulse length limit which is defined by external power supplies. The toroidal component of the magnetic field in RFP is about the same as the poloidal magnetic field. The toroidal magnetic field in RFP is produced by external currents as in tokamaks. It decreases with distance from

the plasma centre and reverses direction near the plasma edge (this fact is reflected in the name of the device). The RFP configuration of the magnetic field is a result of the relaxation process in plasma to a minimal energy state accompanied by conservation of the magnetic helicity (a quantity that measures the field's degree of "twisting"). Thus, magneto-hydrodynamic instabilities (MHD instabilities) and their relaxation play a key role in the construction of RFP equilibria. The resulting RFP magnetic field is weak compared to the two previous concepts and the plasma does not satisfy the Kruskal-Shafranov stability criterion (see Sect. 2.6). This criterion says that the safety factor, defined by (2.1), has to be larger than one at the plasma boundary to keep plasma stable against large scale perturbations driven by the current gradient ($q > 1$). Thus, MHD instabilities not only create the RFP configuration but also destroy plasma confinement in a free boundary case. A conducting shell around the plasma is a way to stabilize the plasma against these perturbations. The motion of the current-carrying plasma due to global instabilities induces currents in the shell and provides a stabilizing restoring force.

In a typical RFP configuration, multiple MHD modes are unstable simultaneously. An overlap of all these perturbations produces a stochastic magnetic field where magnetic field lines wander chaotically inside the plasma. This situation is significantly different to that in tokamaks and stellarators, where the field lines normally stay on their respective flux surfaces and radial transport is suppressed. Stochasticity substantially increases energy and particle transport because particles follow the magnetic field lines going also in the radial direction (not only toroidally and poloidally!). Suppression of the MHD instabilities by reducing the free energy source (the current density gradient) is one of the possible solutions, allowing a reduction of the perturbation level and creation of nested flux surfaces inside the plasma. The other approach is to suppress all instabilities except one and construct the so-called "single helicity state". In this case, a single island dominates and forms nested magnetic flux surfaces with the island helicity inside the plasma. In order to manage these control tasks, RFPs are equipped with a large set of control coils to act on the plasma. Currents in the coils are feedback-controlled, and influence the MHD modes' behavior to control and/or suppress a particular instability. The results of such experiments are very valuable from a scientific point of view and can be used in some cases in tokamaks. In that sense, the RFP is a nice testbed for different control approaches which then can be transferred to the tokamak case. In terms of triple product required for the reactor, the concept is behind modern tokamaks and stellarators as shown in Fig. 2.3. More detailed introduction in to this concept is given in Chap. 9 of "Fusion Physics" book [5].

2.2 Fluid Description of the Plasma

The discussion in the previous section has focused on single particle motion in different magnetic field configurations. Here, we would like to identify basic stability properties of the plasma in a particular magnetic configuration. The self-

consistent interaction between particles in the plasma is extremely important for this problem. Calculation of all interactions between all individual particles is impossible task and is not actually required for plasma physics problems. The macroscopic plasma behavior can be described by averaging over a sufficiently large number of particles, an approach which is also used in statistical mechanics. This formalism leads to a kinetic description of the plasma and the plasma itself is characterized by distribution functions. The kinetic models are very accurate and include a wide variety of physical phenomena which are not interesting for us in this chapter. Thus, a further simplification can be done. Integration of the equation of motion over a distribution function results in the two-fluid description of the plasma while retaining self-consistency in that the electrons and ions form two different fluids (for example see J.A. Bittencourt book “Fundamentals of Plasma Physics” [6]). This fluid model can be simplified further to a single fluid approach which is called magnetohydrodynamics (MHD) and can be also derived by combining Newton’s mechanics and Maxwell’s electrodynamics equations. In its simplest form, the approach treats the plasma as a conductive fluid. The MHD approximation simplifies the problems drastically and substitutes microscopic variables (particle velocities, particle trajectories, etc.) by macroscopic ones, as well as easily recognizable physical quantities (plasma density n , mass density ρ , pressure p , fluid velocity \vec{v} , etc.). This approach is easier to solve and it is more intuitive to understand, in comparison to the kinetic description. The equations of the single-fluid MHD model are the following:

$$\frac{\partial \rho}{\partial t} + \vec{\nabla} \cdot (\rho \vec{v}) = 0 \text{ Conservation of mass} \quad (2.2)$$

$$\rho \frac{d\vec{v}}{dt} = \vec{J} \times \vec{B} - \nabla p \text{ Force balance} \quad (2.3)$$

$$\vec{E} + \vec{v} \times \vec{B} = 0 \text{ (ideal MHD), or } \vec{E} + \vec{v} \times \vec{B} = \eta_{\parallel} \vec{J} \text{ (resistive MHD) Ohm's law} \quad (2.4)$$

$$\nabla \times \vec{E} = -\frac{\partial \vec{B}}{\partial t} \text{ Faraday's law} \quad (2.5)$$

$$\nabla \times \vec{B} = \mu_0 \vec{J} \text{ Ampere's law} \quad (2.6)$$

$$\nabla \cdot \vec{B} = 0 \text{ Absence of magnetic monopoles} \quad (2.7)$$

Here \vec{B} is the magnetic field, \vec{E} is the electric field, \vec{J} is the plasma current density, and η_{\parallel} is the plasma resistivity parallel to the magnetic field. It is important to note that the single fluid MHD approximation does not distinguish between electrons and ions since only their sum appears in the equations; for example, for the plasma pressure $p = p_e + p_i$. The mass density in MHD is clearly

determined by the ions ($\rho \equiv m_i n$) and the momentum of the fluid is carried by the ions as well ($\vec{v} \equiv \vec{v}_i$), because they represent the dominant mass of the plasma.

The equation system is not closed. The typical closure is the adiabatic equation, which represents conservation of energy in the system: $\frac{d}{dt} \left(\frac{p}{\rho^\Gamma} \right) = 0$, where Γ is the adiabatic factor.

The equation system actually contains two different approaches depending on the assumption for the plasma resistivity in Ohm's law. In the case of quasi-static plasma configurations, dissipation rates are small, the plasma resistivity is negligible and the plasma is well described in the frame of ideal MHD ($\vec{E} + \vec{v} \times \vec{B} = 0$). Combining this variant of Ohm's law with Faraday's law results in the convection equation for the magnetic field $\frac{\partial \vec{B}}{\partial t} = \nabla \times (\vec{v} \times \vec{B})$. Thus, evolution of the magnetic field is determined by the plasma motion. The magnetic field is “frozen into” the plasma and any topological changes of the magnetic field in ideal MHD are forbidden.

For long-term evolution of the plasma, non-linear processes with small but finite resistivity become important and the ideal MHD assumption is not valid anymore. Even a small resistivity in the resistive MHD, $\vec{E} + \vec{v} \times \vec{B} = \eta_{\parallel} \vec{J}$, allows to change the topology of the magnetic field at slow resistive time scales² and produces a new class of so-called “resistive” MHD instabilities as discussed later.

The typical fluid approximation is based on the assumption that the system is locally close to the thermodynamic equilibrium, which requires a certain rate of collisions and dissipation (one makes this step at the reduction of the kinetic approach to the fluid description). For that case, the mean free path λ should be short compared with the typical gradient scales, $\lambda |\nabla f| \ll f$ [7]. The mean free path in hot plasmas becomes very long, but at the same time in a magnetized plasma, for perpendicular directions, the mean free path is roughly the gyroradius, $\lambda \approx r_L$. This value is typically very small and the condition is fulfilled. Consequently, the fluid description can be applied to the plasma behavior perpendicular to the magnetic field, which is typically the case for our analysis. In the context of the fusion problem, the MHD model provides a reasonably accurate description of macroscopic equilibrium and stability [8].

2.3 Plasma Equilibrium

The equations which govern the plasma equilibrium can be easily obtained from the system of MHD equations discussed above. For an equilibrium situation, it is naturally to assume zero velocity, $\vec{v} = 0$, and constant macroscopic quantities, $\partial/\partial t = 0$. In this case, the system of equations is reduced to three equations:

² $\tau_R = \frac{\mu_0 l^2}{\eta}$, where η is the plasma resistivity and l is the characteristic width of the reconnection region (see figure 2.7b).

$$\vec{J} \times \vec{B} = \nabla p \quad (2.8)$$

$$\nabla \times \vec{B} = \mu_0 \vec{J} \quad (2.9)$$

$$\nabla \cdot \vec{B} = 0 \quad (2.10)$$

These equations describe the equilibrium properties of all magnetic configurations of our interest.³ The main properties of these configurations can be directly obtained from these equations.

The equilibrium configurations have common properties which are widely used later and which we discuss here before the analysis of plasma stability. Figure 2.4a shows a cross-section of the tokamak plasma. The contours of constant pressure of a well-confined equilibrium form a set of nested surfaces. Two important properties of these surfaces follow directly from the force balance equation. The dot product of the MHD momentum (2.8) with \vec{B} gives:

$$\vec{B} \cdot \nabla p = 0 \quad (2.11)$$

using the fact that $\vec{B} \cdot (\vec{J} \times \vec{B}) = \vec{J} \cdot (\vec{B} \times \vec{B}) = 0$. Thus, the magnetic field lines must lie in the surface of constant pressure because there is no component of \vec{B} perpendicular to the surface (in the direction of the pressure gradient ∇p). The other property is obtained by forming the dot product with \vec{J} :

$$\vec{J} \cdot \nabla p = 0 \quad (2.12)$$

The current lines also lie on the constant pressure surfaces and there is no current component in the direction of the pressure gradient, ∇p . These surfaces of constant pressure and current are also the surfaces of constant magnetic flux, which is a typical “radial” coordinate in fusion devices with arbitrary poloidal cross-section and can be defined using different components of the magnetic field. The toroidal flux definition uses the toroidal magnetic field B_ϕ :

$$\Phi \equiv \frac{1}{2\pi} \int B_\phi dS_\phi. \quad (2.13)$$

The poloidal magnetic flux is defined using the poloidal magnetic field component B_{pol} :

$$\Psi \equiv \frac{1}{2\pi} \int B_{pol} dS_\Psi. \quad (2.14)$$

³ The case of an equilibrium with constant flow does not dominate in fusion configurations and requires a different treatment.

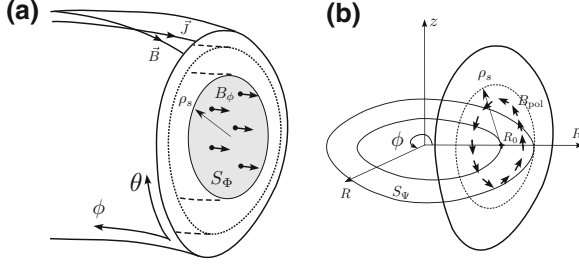


Fig. 2.4 **a** General direction of the \vec{B} and \vec{J} lines on the constant pressure surfaces. The toroidal flux at the position ρ_s is defined using the toroidal magnetic field B_ϕ and the area S_Φ . **b** The definition of the poloidal magnetic flux uses the poloidal magnetic field B_{pol} and area S_Ψ . The magnetic axis is R_0

The respective surfaces are indicated by the shaded areas in Fig. 2.4. Here the normalization factor $(1/2\pi)$ is introduced to simplify the relation between the flux and the poloidal magnetic field:

$$\vec{B}_{pol} = \frac{1}{R} \vec{e}_\phi \times \nabla \Psi \quad (2.15)$$

The safety factor definition (2.1) can be also written using these flux functions:

$$q(\Psi) \equiv \frac{d\Phi}{d\Psi} \quad (2.16)$$

It is convenient to define so-called “radial coordinates”. These values are called poloidal (ρ_{pol}) and toroidal (ρ_{tor}) coordinates depending on the flux used in the definition:

$$\rho_{pol} = \sqrt{\frac{\Psi - \Psi_0}{\Psi_s - \Psi_0}}, \quad (2.17)$$

$$\rho_{tor} = \sqrt{\frac{\Phi - \Phi_0}{\Phi_s - \Phi_0}}, \quad (2.18)$$

where the index s refers to the separatrix and index 0 to the magnetic axis. These coordinates are scaled such that $\rho = 0$ on the magnetic axis and $\rho = 1$ at the plasma boundary.

The equilibrium equations can be also represented conveniently in terms of the flux functions, which leads to so-called Grad-Shafranov equation for the poloidal flux $\Psi = \Psi(R, z)$:

$$R \frac{\partial}{\partial R} \left(\frac{1}{R} \frac{\partial \Psi}{\partial R} \right) + \frac{\partial^2 \Psi}{\partial z^2} = -\mu_0^2 I I' - \mu_0 R^2 p' [= \mu_0 R J_\phi] \quad (2.19)$$

Here, $I \equiv R B_\phi = I(\Psi)$ is the stream function of the poloidal current, which is also a flux function. The prime indicates differentiation with respect to Ψ . The right side of the equation is proportional to the toroidal current density (J_ϕ). The functions $\Psi(R, z)$ and $I(R, z)$ are connected to the plasma current density (J) and the magnetic field as follows:

$$B_R = -\frac{1}{R} \frac{\partial \Psi}{\partial z} B_z = \frac{1}{R} \frac{\partial \Psi}{\partial R} J_R = \frac{1}{R} \frac{\partial I}{\partial z} J_z = -\frac{1}{R} \frac{\partial I}{\partial R} \quad (2.20)$$

The Grad-Shafranov equation can be solved numerically for any plasma cross-section and provides the constant flux (and pressure) surfaces in real tokamak geometry. Detailed derivation of the equation can be found, for example, in the book by J. P. Goedbloed “Advanced magneto-hydrodynamics” [9].

Before we come to the stability analysis, it is important to highlight the two main stabilizing actions of the magnetic field. As was shown before, the conservation of the momentum equation is reduced in an equilibrium situation to a simple force balance between the magnetic force from the current in the plasma, $\vec{F}_{Lorentz} = \vec{J} \times \vec{B}$, and the pressure force, $\vec{F}_{pressure} = -\nabla p$, from the kinetic plasma pressure. This force balance has to be satisfied at each point of the plasma. Two general properties of the magnetic field lines, magnetic pressure and magnetic field line tension, play an important role in this balance (see for example book by Harra and Mason [10]). We formulate the pressure balance in the direction perpendicular to the magnetic field using the force balance (2.8), Ampere’s law for the current \vec{J} , and the vector identity

$$\frac{1}{2} \nabla(B^2) = \frac{1}{2} \nabla(\vec{B} \cdot \vec{B}) = \vec{B} \times (\nabla \times \vec{B}) + (\vec{B} \cdot \nabla) \vec{B}. \quad (2.21)$$

Then the Lorentz force is

$$\vec{F}_{Lorentz} = \vec{J} \times \vec{B} = \frac{1}{\mu_0} (\nabla \times \vec{B}) \times \vec{B} = \frac{1}{\mu_0} \left(\frac{\nabla(B^2)}{2} - (\vec{B} \cdot \nabla) \vec{B} \right) \quad (2.22)$$

$$F_{Lorentz \perp B} = \underbrace{\nabla_\perp \left(\frac{B^2}{2\mu_0} \right)}_{\text{mag.field pressure}} - \underbrace{\frac{B^2}{\mu_0 R_c}}_{\text{mag.field tension} \perp B}. \quad (2.23)$$

The parallel component provides tension only along the magnetic field and is not able to compensate the plasma pressure. The final pressure balance, perpendicular to the magnetic field, can be written as follows:

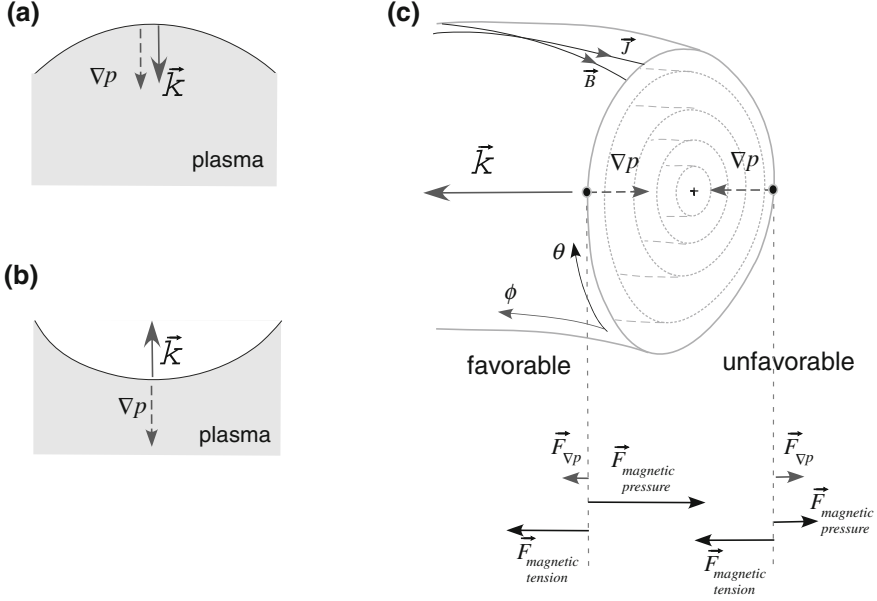


Fig. 2.5 **a** Unfavorable curvature of the magnetic field. **b** Favorable curvature of the magnetic field. **c** The tokamak case has favorable curvature (at the inner side of the torus) and unfavorable curvature (at the outer side of the torus). The resultant equilibrium forces are shown for *low* and *high* field side

$$\nabla_{\perp} \left(\underbrace{\frac{B^2}{2\mu_0}}_{\text{mag.field pressure}} + \underbrace{p}_{\text{plasma pressure}} \right) - \underbrace{\frac{B^2}{\mu_0 R_c}}_{\text{mag.field tension} \perp B} = 0 \quad (2.24)$$

where R_c is the curvature radius. The magnetic field has a property similar to plasma pressure, p , which is the magnetic field pressure, $\frac{B^2}{2\mu_0}$, and the magnetic tension, $\frac{B^2}{\mu_0 R_c}$. The magnetic field line is stretched on a particular flux surface and tries to keep the minimal length due to this tension. In the case where the curvature vector is parallel to the ∇p vector, the curvature is unfavorable and acts as a destabilizer (Fig. 2.5a). As one moves radially outward into the region of larger curvature in Fig. 2.5a, the field tends to become smaller because of the larger radius of curvature. $\langle B^2 \rangle$ decreases indicating instability. The situation is opposite for Fig. 2.5b, where perturbations in the direction of the vacuum region lead to an increase of $\langle B^2 \rangle$ and thus are stabilized. In this case, the curvature vector is antiparallel to the pressure gradient vector, and the system has so-called “favorable curvature”. This result can be obtained also from changes of the system energy due to a perturbation in these

two cases (see 2.35). The real tokamak situation is more complicated and has both types of the curvatures (Fig. 2.5c). In this case, decay of the magnetic field has to be taken into account ($B \sim 1/R$) together with local magnetic field curvature (R_c) for radial pressure balance.

The combination of the magnetic field pressure gradient, $\nabla_{\perp} \left(\frac{B^2}{2\mu_0} \right)$, and the magnetic field tension, $\frac{B^2}{\mu_0 R_c}$, gives a resultant force, which counteracts plasma pressure force, $F_{\nabla p} = -\nabla_{\perp} p$, and provides radial force balance (Fig. 2.5c). At the low field side, the magnetic field tension provides plasma stability, while the gradient of the magnetic field pressure makes the plasma stable on the high field side. Thus, the resultant Lorentz force counteracts the plasma pressure gradient at each point on the flux surface. This force is larger at the inner side of the torus (favorable region) and lower at the outer side of the torus (unfavorable region). The net effect can be determined only by careful numerical analysis for a particular plasma configuration. At the same time, the basic idea to keep more plasma at the favorable curvature region leads to elongated and D-shaped plasma cross-section in modern tokamaks. This shape provides a natural way for X-point formation and divertor operations as will be discussed later.

2.4 Plasma Stability

The main question in the MHD stability theory is to consider an MHD equilibrium and predict its stability. Plasma stability with respect to different perturbations can be analyzed in several different ways. Here, we restrict our consideration to the simplest form of the energy principle within the ideal MHD approximation. The perturbations are assumed to be small in comparison to equilibrium quantities, for example pressure perturbations are much less than the pressure value, $p_1 \ll p_0$. In the following, equilibrium quantities and perturbed quantities are denoted by subscript 0 and 1, respectively. This assumption, together with the assumption of the stationary equilibrium state ($\vec{J}_0 \times \vec{B}_0 = \nabla p_0$, $\vec{v}_0 = 0$) lead to a system of linearized MHD equations:

$$\frac{\partial \rho_1}{\partial t} + \rho_0 \vec{\nabla} \cdot \vec{v}_1 = 0 \quad (2.25)$$

$$\rho_0 \frac{d\vec{v}_1}{dt} = -\nabla p_1 + \vec{J}_0 \times \vec{B}_1 + \vec{J}_1 \times \vec{B}_0 \quad (2.26)$$

$$\frac{\partial p_1}{\partial t} = -\vec{v}_1 \cdot \nabla p_0 - \Gamma p_0 \nabla \cdot \vec{v}_1 \quad (2.27)$$

$$\frac{\partial \vec{B}_1}{\partial t} = \nabla \times (\vec{v}_1 \times \vec{B}_0) \quad (2.28)$$

$$\nabla \times \vec{B}_1 = \mu_0 \vec{J}_1 \quad (2.29)$$

$$\nabla \times \vec{B}_0 = \mu_0 \vec{J}_0 \quad (2.30)$$

We use these equations to identify energy changes in the system resulting from small initial perturbations. The energy principle is based on the idea that an equilibrium is unstable if any perturbation reduces the potential energy of the system. Changes in the potential energy can be calculated for an arbitrary displacement, $\vec{\xi}$, using the system of MHD equations. The displacement is directly related to the plasma velocity, $\vec{v}_1 = \frac{d\vec{\xi}}{dt}$. The system of linearized MHD equations can be rewritten in the form of the wave equation:

$$\begin{aligned} \vec{F}(\vec{\xi}) \equiv \rho_0 \frac{\partial^2 \vec{\xi}}{\partial t^2} = & J_0 \times \left[\nabla \times (\vec{\xi} \times \vec{B}_0) \right] + \frac{1}{\mu_0} \left\{ \nabla \times \left[\nabla \times (\vec{\xi} \times \vec{B}_0) \right] \right\} \times \vec{B}_0 + \\ & \nabla (\vec{\xi} \cdot \nabla p_0) + \Gamma \nabla (p_0 \nabla \cdot \vec{\xi}) \end{aligned} \quad (2.31)$$

This equation is the ideal MHD wave equation, which defines the ideal MHD force operator $\vec{F}(\vec{\xi})$. The same conclusion can be obtained starting from the force balance (2.8). If the plasma is unstable, the force balance is not fulfilled and the resulting force is non-zero:

$$\vec{F}_{result} = \vec{J} \times \vec{B} - \nabla p \neq 0 \quad (2.32)$$

We can substitute this force into Newton's second law, where the second derivative of the displacement gives the plasma acceleration, $\vec{a} = \frac{\partial \vec{v}}{\partial t}$. The resulting equation is identical to the previous result if one substitutes total values of the current, pressure and magnetic field and makes the linear MHD assumption:

$$\rho \frac{\partial^2 \vec{\xi}}{\partial t^2} = \vec{F}_{result}(\vec{\xi}) = \vec{J} \times \vec{B} - \nabla p = \vec{F}(\vec{\xi}) \quad (2.33)$$

This resulting force operator can be used directly to calculate changes in the potential energy of the plasma as an integral over the whole system volume (including the plasma region, the vacuum region and the conducting wall):

$$\delta W = \int \vec{\xi} \cdot \vec{F}(\vec{\xi}) dV \quad (2.34)$$

If the energy change is positive, the plasma is linearly stable with respect to the perturbation $\vec{\xi}$ ($\delta W \geq 0$), otherwise the plasma is unstable ($\delta W < 0$). It is convenient to write this equation in the so-called “intuitive form” [8, 11].

$$\delta W = \delta W_{plasma} + \delta W_{vacuum} + \delta W_{surface} \quad (2.35)$$

$$\delta W_{plasma} = \frac{1}{2} \int_{plasma} \left\{ \frac{|\vec{B}_{1,\perp}|^2}{\mu_0} + \frac{B_0^2}{\mu_0} \left| \nabla \cdot \vec{\xi}_\perp + 2\vec{\xi}_\perp \cdot \vec{\kappa} \right|^2 + \Gamma p_0 \left| \nabla \cdot \vec{\xi} \right|^2 - 2 \left(\vec{\xi}_\perp \cdot \nabla p_0 \right) \left(\vec{\kappa} \cdot \vec{\xi}_\perp^* \right) - J_\parallel \left(\vec{\xi}_\perp^* \times \hat{b} \right) \cdot \vec{B}_{1,\perp} \right\} dV$$

$$\delta W_{vacuum} = \frac{1}{2} \int_{vacuum} \frac{(B_1)^2}{\mu_0} dV$$

$$\delta W_{surface} = \frac{1}{2} \int_{surface} \left| \vec{n} \cdot \vec{\xi}_\perp \right|^2 \vec{n} \cdot \left\| \nabla \left(p + \frac{B^2}{2\mu_0} \right) \right\| dS$$

$$\vec{B}_1 = \vec{B}_{1,\perp} + B_{1,\parallel} \hat{b}, \quad B_{1,\parallel} = -B_0 \left(\nabla \cdot \vec{\xi}_\perp + 2\vec{\xi}_\perp \cdot \vec{\kappa} \right) + \frac{\mu_0}{B} \vec{\xi}_\perp \cdot \nabla p_0, \quad \vec{J} = \vec{J}_\perp + J_\parallel \hat{b},$$

$\vec{\xi} = \vec{\xi}_\perp + \xi_\parallel \hat{b}$, $\vec{\kappa} = \hat{b} \cdot \nabla \hat{b}$, where the indexes \parallel and \perp refer to the direction parallel and perpendicular the equilibrium magnetic field B_0 , perturbed magnetic field is expressed as $\vec{B}_1 = \nabla \times (\vec{\xi} \times \vec{B}_0)$, and $\|T\|$ denoting the jump in T from vacuum to plasma.

The squares of all components are always positive and provide only stabilizing effect on the plasma:

- (1) $\frac{|\vec{B}_{1,\perp}|^2}{\mu_0} > 0$ is *stabilizing* because the magnetic field tries to prevent its bending;
- (2) $\frac{B_0^2}{\mu_0} \left| \nabla \cdot \vec{\xi}_\perp + 2\vec{\xi}_\perp \cdot \vec{\kappa} \right|^2 > 0$ is *stabilizing* because the magnetic field tries to prevent its compression;
- (3) $\Gamma p_0 \left| \nabla \cdot \vec{\xi} \right|^2 > 0$ is *stabilizing* because the plasma itself counteracts compression (Γ is the adiabatic factor)
- (4) $2 \left(\vec{\xi}_\perp \cdot \nabla p_0 \right) \left(\vec{\kappa} \cdot \vec{\xi}_\perp^* \right)$ can be either positive (stable) or negative (*unstable*). The term depends on the pressure gradient and can lead to the so-called “pressure-driven” instabilities. As discussed before, this term is typically more unstable at the low field side of the tokamak.
- (5) $J_\parallel \left(\vec{\xi}_\perp^* \times \hat{b} \right) \cdot \vec{B}_{1,\perp}$ can be also either stable or *unstable*. It gives rise to the so-called “current-driven” instabilities if it is negative. Instabilities are driven by the parallel component of the current.

There is an important factor which can influence the MHD stability and is not considered in the MHD approximation. MHD instabilities can interact directly with some of the plasma particles. This process has a kinetic nature and requires more complicated approaches than MHD for a correct description. These particle-wave interactions have either a “resonant” or a “non-resonant” character. MHD instability is a perturbation of the plasma which is characterized by plasma displacement and also by perturbed electric and magnetic fields associated with this displacement. Thus, the instability can be considered as an electromagnetic wave with a particular phase velocity. The particles with similar velocities will be either accelerated or decelerated. Depending on the initial slope of the particle distribution function and its spatial gradient the net result could either make the mode unstable (energy transfer from particle to the instability) or make it more stable (energy flows from the instability into particle motion). This is an example of resonant interaction. If the particles are much faster than the frequency of the wave, they enclose a certain magnetic flux within their orbit. Conservation of this flux tries to prevent any external distortions (any displacement due to MHD instability) and stabilize the instability. This is an example of the “non-resonant” interaction. Results of all these kinetic processes are mentioned in this chapter as “particle-driven” instabilities.

The safety factor value, introduced in (2.1) and (2.16), is a relation between toroidal and poloidal flux changes which defines the inclination of the magnetic field lines at a particular flux surface, or how fast the magnetic field line winds around the torus. Neighboring flux surfaces have different inclination of the magnetic field lines and thus different safety factor values. Simple analysis shows that two situations are possible for the field line behavior at a flux surface depending on its safety factor value:

- (1) The magnetic field line winds around the corresponding flux surface and never ends. In this case it covers densely the whole flux surface and the surface is “non-resonant” (Fig. 2.6a).
- (2) The field line closes after a few windings around the torus if the safety factor at this flux surface can be represented as relation between two co-prime integers: $q = m/n$. In contrast to the previous situation, the field line does not densely cover the flux surface and perturbations are easily excited here. These surfaces are called “resonant surfaces”. A perturbation with the same helicity as the resonant surface can occur here, with the poloidal mode number m and toroidal mode number n .

There is a wide variety of MHD instabilities which can be unstable inside the plasma or at the plasma boundary. These modes limit maximal achievable plasma parameters and the main properties of these modes have to be studied carefully. We start this study with a classification of the MHD instabilities in the next section.

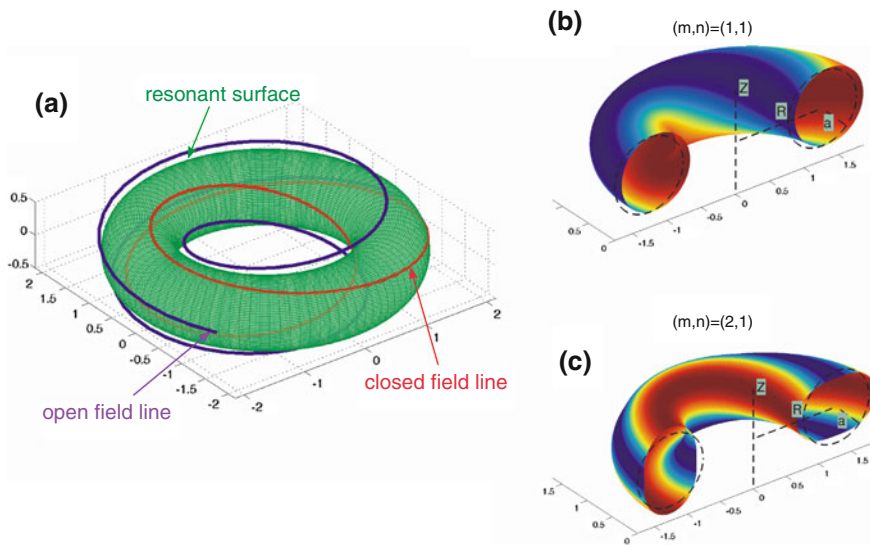


Fig. 2.6 **a** Resonant surface (green) and corresponding closed field line (red). The neighboring flux surface is non-resonant and the field line is open (blue). **b** Displacement of the flux surface due to an $(m,n) = (1,1)$ perturbation. The dashed line represents the undisturbed contour. **c** Displacement of the flux surface due to an $(m,n) = (2,1)$ perturbation. The dashed line represents the undisturbed contour

2.5 Basic Classifications of MHD Instabilities

There are several basic values which can be measured in the experiment and characterize MHD instability in tokamaks:

- growth rate of the mode (γ),
- mode numbers (m,n) ,
- mode frequency in the laboratory frame (ω),
- radial structure of the eigenfunction $(\hat{\xi}_r(\rho))$, where ρ is the radial coordinate.

The growth of the mode amplitude is typically characterized by the growth rate (γ) assuming the exponential growth of the perturbation with time ($b(t) = \hat{b}_r e^{\gamma t}$).⁴ The instability with mode numbers (m,n) has the same helicity as the resonant surface where it is located. Thus, the safety factor value of the resonant surface follows directly from the helical structure of the instability ($q = m/n$). If the mode

⁴ The exponential growth is assumed in linearized MHD (2.25)–(2.30). It is called “linear growth” phase. This description is applicable only in some special cases, for example for resistive wall modes dynamic in RFPs. In practice, the modes are often in non-linear regime and this assumption is not valid anymore, for example for tearing modes, edge localized modes, etc.

rotates with respect to the laboratory frame, its rotation is characterized by the mode frequency (ω). The structure of the radial displacement component ($\hat{\xi}_r(\rho)$) represents the shift of the equilibrium flux surfaces due to the perturbation at different radial locations. Identification of all these values, in particular the radial structure of the displacement, is a challenging task which is described in Chap. 3. If all these values are known, one can describe the displacement of the equilibrium due to a stationary mode in each point of the plasma:

$$\xi(\rho, \theta, \phi, t) = \hat{\xi}_r(\rho) \cdot \cos(m\theta - n\phi + \omega t) \cdot e^{it} \quad (2.36)$$

Examples of the distorted surfaces due to perturbations with $(m, n) = (1, 1)$ and $(m, n) = (2, 1)$ helicities are shown in Fig. 2.6b, c respectively.

Up to this point, only the structure of the instability has been discussed. It is an important ingredient for basic classification of the MHD instabilities based on its physical properties. In order to classify an instability, one has to answer three main questions:

- (1) What is the dominant drive for the instability? Typical possibilities are: “current-driven”, “pressure-driven” and “particle-driven” instabilities.
- (2) Is the instability “resistive” or “ideal”? In case of an ideal instability, the flux surfaces in the plasma are preserved, the instability changes only the shape of the surfaces (Fig. 2.7a). It grows with the Alfvénic time ($\gamma \sim \frac{1}{\tau_A}$, $\tau_A = \frac{a}{v_A}$, $v_A = \sqrt{\frac{B^2}{\mu_0 m_i n}}$, where n is the plasma density and a is the characteristic length of the instability). This time is very short and ideal instability poses ultimate limits for plasma confinement. These instabilities are called “kink” instabilities because the plasma displacement due to such an instability tilts and kinks the plasma. Ideal MHD, which implies zero resistivity, preserves the plasma topology and is sufficient to describe the process. The so-called “resistive instabilities” requires changes of the field line topology. These changes appear only in a small part of the plasma volume, in the X-points (Fig. 2.7b). In these regions the plasma resistivity cannot be neglected and leads to topological changes. These small regions have a dramatic influence on the global equilibrium. The plasma gets access to a new degree of freedom and tries to find the minimal energy state without topological limitations. The time scale for the resistive instability is a mixture between slow resistive diffusion time ($\tau_R = \frac{\mu_0 l^2}{\eta}$, where η is the plasma resistivity and l is the characteristic width of the reconnection region, $l \ll a$) which reflects the topological changes, and fast dynamics of the plasma (τ_A). The typical manifestations of such modes in a tokamak are tearing modes (TMs) and neoclassical tearing mode (NTMs). The name implies tearing and reconnection of the magnetic field lines.
- (3) Where is the dominant location of the instability? Typically, each instability develops predominantly either inside the plasma (internal mode, $\xi(a) = 0$) or

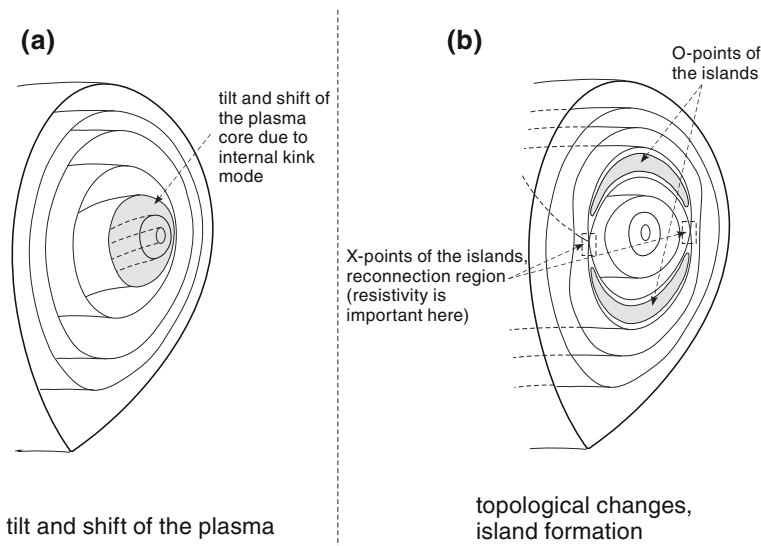


Fig. 2.7 **a** Ideal MHD instability. Internal kink mode is shown **b** Resistive MHD instability. Tearing mode is shown

at the plasma boundary (external mode/free boundary mode, $\zeta(a) \neq 0$). In tokamak plasma, different modes with the same toroidal mode number n are coupled. These secondary modes, with mode numbers $(m \pm 1, n)$, have components at the plasma surface even if the dominant mode (m, n) is purely internal. In some cases, this can be neglected and one assumes the mode to be internal (Plasma shaping gives additional coupling to other poloidal mode numbers).

The presented classification is shown in Fig. 2.8. It is important to note that this classification is very basic. The toroidal geometry of tokamaks, non-circular cross-section and other effects lead to a mixture of different modes which are unstable simultaneously, for example coupling between external and internal modes. Situations with combined drives or with changes of the dominant drive are also possible, for example a current-driven classical tearing mode TM converts into a pressure-driven neoclassical tearing mode NTM when the size of the mode becomes sufficiently large and the plasma pressure is sufficient. All these complicated cases have to be studied carefully both experimentally and numerically. Nevertheless, the presented simple classification allows to get a basic idea about the problem and provides a preliminary case characterization. It is important to note that the zoo of MHD instabilities in the plasma is extremely large. All instabilities have particular names, many of them are connected to the historical background, not to the physical properties. We have considered keeping the number of names at a minimal possible level and forwarding the readers to other books with detailed descriptions, for example: A.B. Mikhailovskii "Instabilities in a confined plasmas" [12].

Basic classification of MHD instabilities

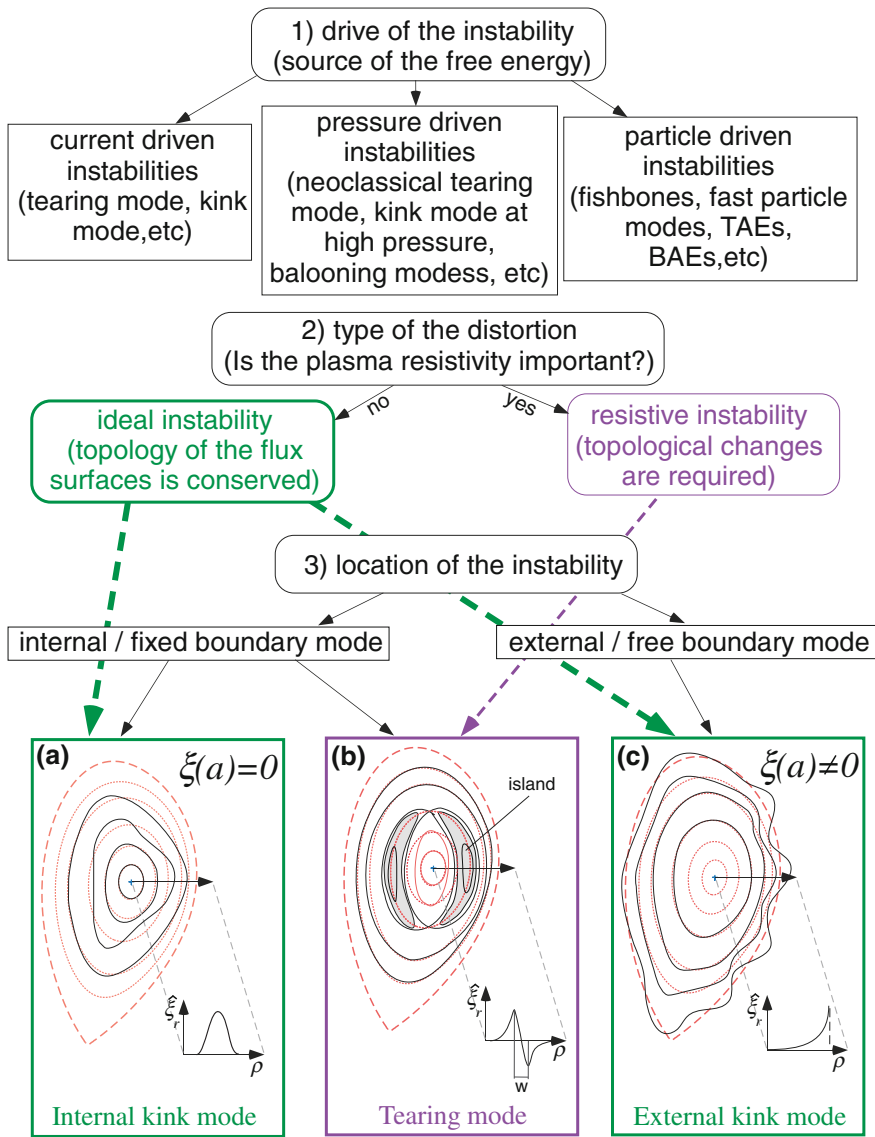


Fig. 2.8 The basic classification of MHD instabilities

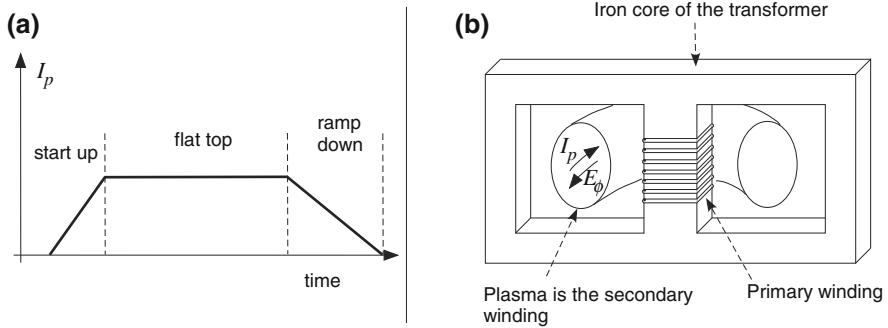


Fig. 2.9 **a** Plasma current time trace and different phases of the discharge. **b** Tokamak startup. Plasma acts as the secondary winding of the transformer. External voltage is applied on the primary winding

2.6 Hugill Diagram

The first step for fusion device operation is the plasma production. In a tokamak, the primary toroidal magnetic field is produced at the first step. Then the vacuum vessel is filled with a gas. Typical choice for the gas is either a hydrogen isotope (H, D, T) or helium. This gas has to be heated and ionized to become plasma during the start-up phase when the plasma current rises, which is typically achieved using a transformer for the tokamak start-up (Fig. 2.9).

Changes in the voltage applied at the primary winding of the transformer induce a toroidal electric field inside the vacuum vessel filled with gas. Some free electrons are almost always present in a tokamak chamber, but can be also produced, for example by external electromagnetic waves. These electrons are accelerated by the electric field, and insofar as the electron has an energy higher than the ionization energy of the gas, it can ionize a neutral atom, which releases an additional electron. These electrons can be accelerated by the electric field and produce more electrons in an avalanche process. Thus, toroidal current in the plasma rises and the plasma plays the role of the second winding of the transformer. The gas puff and the transformer voltage are two main parameters which can be controlled externally during start-up of the plasma and later in the flat top phase of the discharge. The gas puff strongly influences plasma density and the loop voltage at the primary winding is linked to the plasma current. It is important to note that these two parameters are not independent. A particular plasma current can be achieved only for a given range of the plasma densities and stable operation is possible only in a restricted area in the (I_p, n_e) space, shown in the so-called Hugill diagram (Fig. 2.10). If the stability boundary is crossed, the discharge is either terminated abruptly (plasma disruption, hard limit), or the plasma confinement degrades over a longer time (soft limit).

There are three main stability boundaries on this diagram: (i) runaway limit, (ii) current limit, and (iii) Greenwald limit. All together they define the stable operation space in terms of the plasma current and average plasma density. This

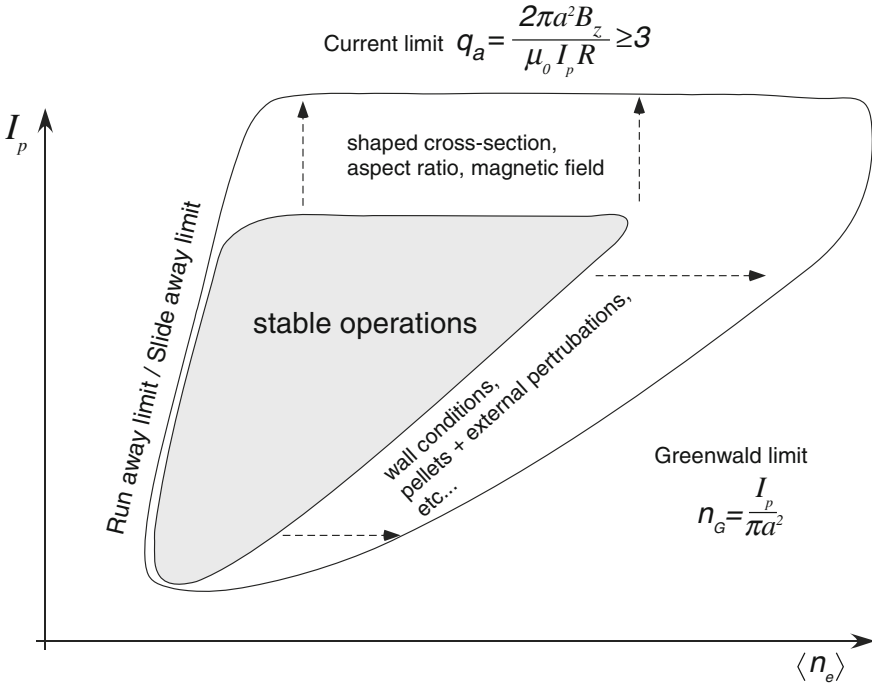


Fig. 2.10 The Hugill diagram and the main limits for plasma operations

diagram does not present all limitations for the plasma operations, but provides a general idea regarding possible parameters.

The *runaway* (or *slideaway* limit) is near the left border of the graph at low plasma density. As discussed before, plasma electrons are continuously accelerated by the toroidal electric field. If an electron gains more energy per toroidal turn than it loses by collisions in low density plasma, it does not transfer the energy to the plasma ions anymore. Operation close to this limit is not very interesting for two reasons:

- the fusion reactor requires higher density operation for higher fusion performance, which is not the case in this regime;
- the lost electrons may cause damage of the first wall.

The other two limits are more important and we discuss them in detail.

2.6.1 Current Limit

The maximum current limit of a tokamak depends on many different factors and has to be calculated numerically, but main ideas can be derived from simple MHD models. The simplest MHD model for a tokamak is the “straight tokamak”

approximation, a column of plasma having a circular cross-section and length $L = 2\pi R_0$. The fields have to satisfy the tokamak inverse ratio expansion $B_\theta/B_Z \sim \varepsilon = a/R_0 \ll 1$, and periodic boundary conditions. In this case, Z is the “toroidal” coordinate along the plasma cylinder instead of ϕ and r is the radial coordinate of the plasma column. These assumptions exclude any influence of the toroidicity on the problem and provide an estimation for the current-driven modes. The most dangerous instabilities in the “straight tokamak” are external kink modes, which have resonant surfaces outside the plasma boundary, in the vacuum region. The energy changes due to such an instability, with poloidal and toroidal mode numbers (m, n) , can be estimated using the energy principle (2.35), which takes into account the “straight tokamak” simplifications and can be written in the following form [8, 13, 14]:

$$\begin{aligned} \delta W = & \underbrace{\frac{2\pi^2 B_z^2}{\mu_0 R_0} \int_0^a \left(\left(r \frac{d\xi_r}{dr} \right)^2 + (m^2 - 1) |\xi_r|^2 \right) \left(\frac{n}{m} - \frac{1}{q} \right)^2 r dr}_{\text{plasma}} \\ & + \underbrace{\frac{2\pi^2 B_z^2}{\mu_0 R_0} \left(\frac{2}{q} \left(\frac{n}{m} - \frac{1}{q} \right) + \underbrace{(1 + m\lambda) \left(\frac{n}{m} - \frac{1}{q} \right)^2}_{\text{wall}} \right) r^2 |\xi_r|^2}_{\text{vacuum}} \bigg|_{r=a} \end{aligned} \quad (2.37)$$

where $\lambda = \frac{1+(a/b)^{2m}}{1-(a/b)^{2m}}$ represents the influence of the wall at radius b .

The first part of the expression is the integral from the plasma center, $r = 0$, to the plasma boundary $r = a$. All terms under the integral are positive. Thus, if the wall is at the plasma boundary, the system is stable.⁵ The second part describes the vacuum region and influence of the conducting wall, $a < r < b$. The effect of the wall is represented by the second term in the vacuum part. This contribution is also stabilizing, because $\lambda > 1$ and this term is always positive. The only potentially unstable contribution comes from the first term in the vacuum part. It gives a destabilizing contribution if the following relation holds:

$$\left(\frac{n}{m} - \frac{1}{q} \right) < 0 \quad (2.38)$$

Thus, the necessary condition for the mode to be unstable is $q_a < m/n$, and the resonant surface is in the vacuum region in this case. Potentially, the most unstable external kink mode has poloidal and toroidal mode numbers $(m, n) = (1, 1)$, and

⁵ The plasma part of the system is stable only in the ε^2 order. In case of the $(m, n) = (1, 1)$ internal kink mode, the plasma integral is zero and higher order expansion has to be taken into account, see for example Bussac et al., Phys. Rev. Lett. Vol 35, p. 1638.

the stability condition for the safety factor at the plasma boundary is $q_a > 1$. This condition is called the Kruskal-Shafranov limit for the plasma current because the edge safety factor is directly related to the plasma current:

$$q_a = \frac{2\pi a^2 B_Z}{\mu_0 I_p R} \text{ (“straight tokamak” model)} \quad (2.39)$$

In reality, stable operations require higher values of the edge safety factor ($q_a \geq 3$) and the maximum plasma current is strongly limited. Special, non-circular plasma cross-sections can improve the situation. The D-shaped cross-section, which is used in all modern tokamaks, utilizes the combined effect of the plasma elongation and triangularity. This shape naturally allows higher plasma currents for a given aspect ratio and magnetic field. Stability of the kink modes in real tokamaks is investigated numerically taking into account real plasma geometry, the current and the pressure profiles. If the kink mode is unstable, it leads to a strong and fast deformation of the plasma boundary and the plasma disrupts (hard limit).

2.6.2 Greenwald Limit

To the right of the operation space we encounter the density limit, which determines maximum achievable plasma density for a given plasma current. This is the most interesting corner of the operation space, since the fusion reaction rate scales with n^2 . The plasma current has to be also maximised to reach this goal as seen from Fig. 2.10. In the majority of cases, the density limit shows up as a disruptive event in which the plasma thermal energy is quenched in about 1 ms, while the energy stored in the plasma current is dissipated on a time scale of the order of 10 ms [15]. The most common relation for the density limit is the empirical scaling, so-called Greenwald limit:

$$n_G = \frac{I_p}{\pi a^2} \quad (2.40)$$

where n_G is the line average density in units of 10^{20} m^{-3} , I_p is the plasma current in MA, and a is the minor radius in m . The presented formulation describes relatively well the limits for circular and shaped plasma cross-sections (Fig. 2.11) [16, 17].

Unlike the current limit, which depends on MHD physics alone, the density limit physics includes transport and atomic processes. The general picture of the density limit involves edge cooling followed by the current profile shrinkage. The current profile becomes unstable with respect to tearing and/or kink modes and the plasma becomes stochastic and cold. Typical manifestations of this process is multifaceted asymmetric radiation from the edge (MARFE), which creates a toroidally symmetric zone of high radiation either at the high field side (limiter) or

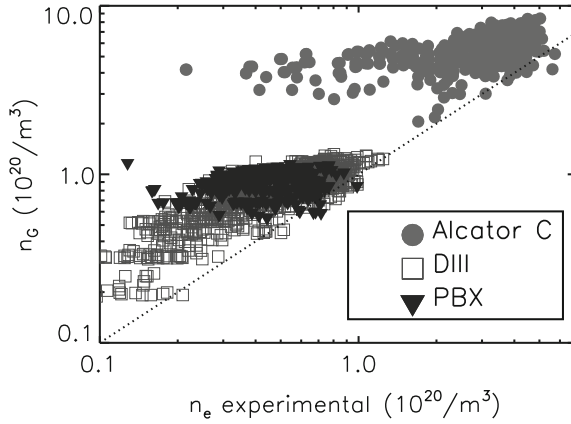


Fig. 2.11 Recorded densities versus Greenwald predictions in circular and shaped tokamaks. (The figure is from [16]. All rights reserved.)

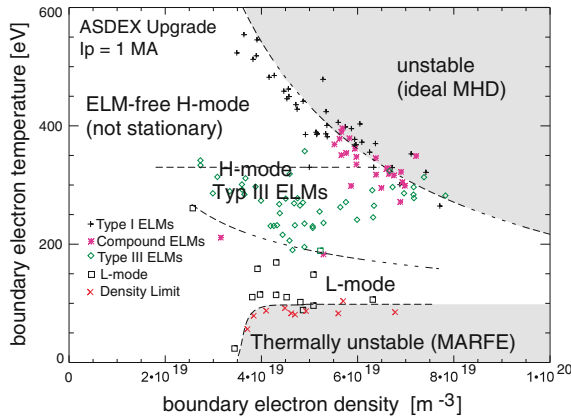
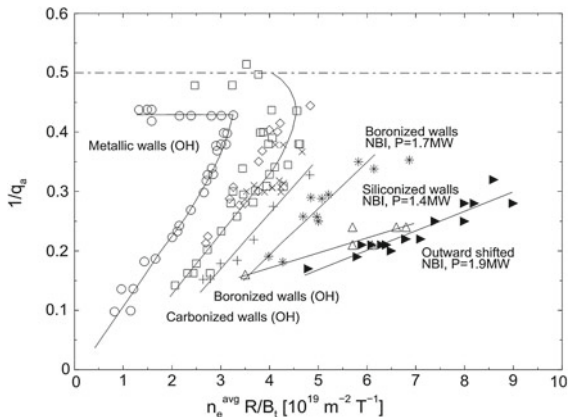


Fig. 2.12 Operation space of the ASDEX Upgrade tokamak is represented in terms of the edge plasma parameters. The density limit occurs when the edge temperature falls below a threshold and plasma goes into a thermally unstable regime (MARFE regime) (The figure is from [19]. All rights reserved.)

around the separatrix X-point (divertor) [15, 18]. The origin of the density limit is not yet fully understood, but the main findings show strong connection to the edge plasma physics. This idea is supported by the fact that the operation regimes can be defined in terms of edge temperature and density (Fig. 2.12) [19]. Here, the density limit occurs when the edge temperature falls below a threshold and plasma goes into a thermally unstable regime (MARFE regime). The electron temperature in this region is very low and the electron density becomes very high. The line radiation due to ionization and charge exchange of the incoming neutral particles provide the largest part of the energy losses.

Fig. 2.13 Hugill diagram for the TEXTOR tokamak with different wall conditioning and different heating scenarios. Advanced wall coating methods extend the operation space (The figure is from [20])



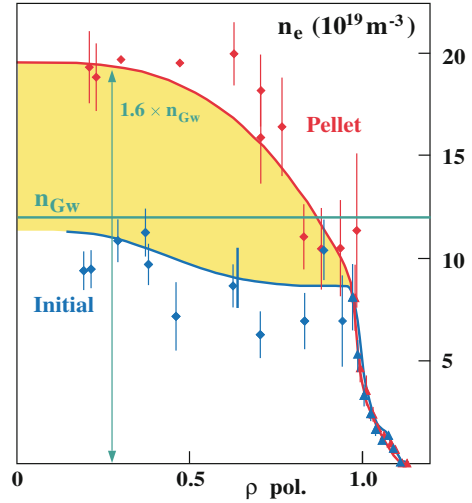
There are several ways to extend the density limit. The achievable density is clearly reduced if the plasma is contaminated by impurities. Wall conditioning is a standard technique to avoid this situation. An example is presented in Fig. 2.13 for the TEXTOR tokamak. Different groups of data points in Fig. 2.13 show that the limit has increased due to the application of advanced wall coating methods: carbonized wall, boronized wall, and siliconized wall [20].

The basic idea is that the impurities released at the first wall can dilute the plasma and cause strong line radiation. The disruption becomes unavoidable when the total radiated power exceeds the heating power. Any action against this scenario helps to keep the plasma healthy and improves the situation. For example, additional heating permits higher radiation losses and enhances the density limit. Unfortunately, the situation is more complicated and increase in power not always helps. Generally, the density limit is not found to increase strongly with input power [16]. This is in clear contradiction to the simple power balance model.

The other way to increase the density well above the Greenwald limit in present experiments is pellet fueling (Fig. 2.14). Results from the ASDEX Upgrade tokamak show that pellet fueling in combination with magnetic fields from active in-vessel saddle coils allow to sustain very attractive plasma scenarios. In this case, core densities up to $1.6n_G$ have been reached while maintaining mitigation of dangerous big edge localized modes (ELMs) [21].

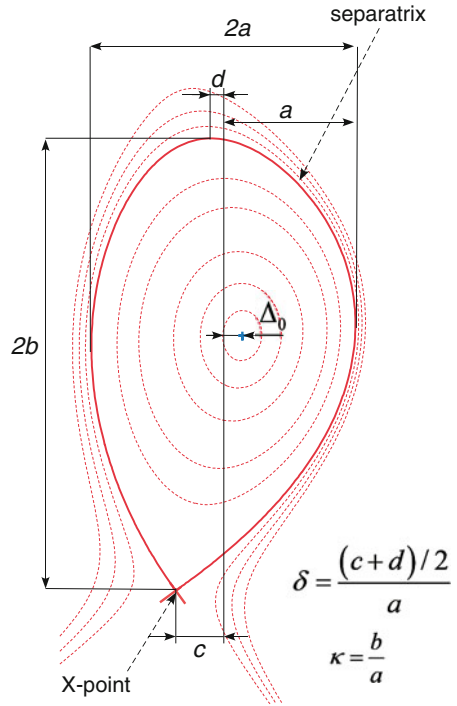
There are also other factors which influence the density limits; for example, plasma triangularity has been found to be important in determining the density at which confinement begins to drop. This is probably connected to the pedestal stability, which depends on the plasma shape. There are several ideas which try to explain the mechanism for the onset of the density limit. For example, the theory of D.A. Gates and L. Delgado-Aparicio assumes that the onset of the density limit is the same as the onset criterion for radiation-driven islands. One can reproduce the density scaling using this assumption [22]. This theory provides a nice explanation for cases with radiation from the island, but it has difficulties to explain cases when radiation from the islands is not observed.

Fig. 2.14 Density profiles in ASDEX Upgrade with and without pellet fueling are shown. Greenwald density limit is marked by green line. The density is well above Greenwald limit in the plasma core but is less than this limit at the plasma edge (The figure is from [21]. © IAEA. All rights reserved)



Operations in other fusion devices are also limited by the density limit. In reversed field pinches, the density limit is the same as in tokamaks. Situation in stellarators is completely different. This device has intrinsically no current which makes the plasma more calm. In order to apply the Greenwald formula the helical winding of the field lines in stellarator should be converted into equivalent plasma current (2.39). The result data points from present stellarators clearly exceed the Greenwald limit and show no indications for “absolute” limits. Operation limit is typically set by radiative/thermal instabilities. Density limit for stellarators approximately obeys Sudo scaling $n_c \sim (PB/V)^{0.5}$, where P is the heating power, B is the magnetic field and V is the plasma volume [23], with densities up to 5 times the Greenwald limit. Exceeding the density limit in stellarator leads to degradation of the plasma confinement on a transport time scales, which is much longer compared to fast disruptive MHD instabilities in tokamaks. Thus, the two main advantages of the stellarator concept are higher density limit and absence of dangerous disruptive instabilities. The reason for two different density scalings is not clear. It could be either a different physics in the machines with and without plasma current or wrong interpolation for the effective plasma current in stellarator case. In spite of the long history of the density limit, there is no widely accepted first principle theory which can explain it. It has to be noted that the density and current limitations of Hugill diagram give basic limitations for plasma operation. Other limits, which are not covered by a simple $(I_p, \langle n \rangle)$ diagram, will be discussed in the next subsections.

Fig. 2.15 Plasma shape of a typical ASDEX Upgrade discharge is shown. Main characteristics are: elongation (δ), triangularity (κ) and Shafranov shift (Δ)



2.7 Restriction Due to Plasma Shaping

Modern tokamaks have strongly non-circular, D-shaped plasma cross-sections in the poloidal plane (Fig. 2.15).

This shape is characterized by two main dimensionless quantities:

- (1) plasma elongation

$$\kappa = \frac{b}{a} \quad (2.41)$$

- (2) plasma triangularity⁶

$$\delta = \frac{(c+d)}{2a} \quad (2.42)$$

The flux surfaces are shaped and shifted due to the Shafranov shift, Δ_0 , which is the result of the force balance and comes directly from the solution of the Grad-Shafranov (2.19). The other important feature is the X-point. The poloidal magnetic field, B_θ , is zero at the X-point. In its vicinity, the magnitude of the poloidal magnetic

⁶ In praxis, also upper triangularity, $\delta_u = d/a$, and lower triangularity, $\delta_l = c/a$, are used.

field is proportional to the distance from the X-point. Thus, the field lines in the X-point region have almost all their trajectories close to the X-point and the separatrix safety factor $q \rightarrow \infty$. Instead of this value, for practical purposes, the values q_{95} , q_{98} , and q_{99} are used. These values are safety factor values at the flux surfaces, which enclose 95, 98, and 99 % of the total magnetic flux respectively.⁷ The shape of the last closed flux surface can play an important role for free boundary instabilities; in this case the flux cut is made at higher values, for example at 99,98 %.

The D-shape plasma cross-section has two main advantages in terms of plasma confinement: (i) it increases the current limit, which allows higher plasma current for the same aspect ratio and toroidal magnetic field; (ii) it leads to natural separatrix formation, and hence operation in high confinement mode (H-mode) with divertor. The exact plasma stability boundaries in such configurations require numerical analysis with elaborated code packages (for example [24–26]), but the main points of the stability analysis can be shown on a simple basis.

The possible plasma shape has several basic limitations. The first limitation is the maximum possible plasma elongation. The plasma with circular cross-section is neutrally stable with respect to toroidally symmetric vertical motion, toroidal mode number $n = 0$, in the inhomogeneous magnetic field of the tokamak. If the plasma is elongated, it can be unstable to a motion in the direction of the elongation. Stability of the plasma, in the simple case of large aspect-ratio plasma without stabilizing conductors, is determined by the magnetic field decay index, which has to be positive:

$$n_v = -\frac{R}{B_Z} \frac{dB_Z}{dR} > 0, \quad (2.43)$$

where B_Z is the externally applied vertical magnetic field (discussed in the next section). R is the major radial coordinate. A conducting wall and internal conducting structures inside the device change stability properties and numerical calculations are required for practical cases.

If this stability criterion is violated, then in the absence of any wall or other conducting structure surrounding the plasma, instability occurs on a fast inertial time scale. However with surrounding conducting structures then there is a range of $n_v < 0$ in which the growth is slowed to the resistive decay time of the surrounding structures. The vertical instability can be controlled by active feedback stabilization system up to an elongation $\kappa = 2.2$ [27]. At the same time, the practical limit for modern tokamaks with relatively close conducting shells is about $\kappa \approx 1.8$ [28].

The second limitation comes from ballooning and kink modes. It was shown that proper choice of the plasma elongation and triangularity brings the plasma into a stable operation window even at high pressure as discussed in the next section.

⁷ This is different to the limiter plasma where the safety factor at the plasma edge, q_a , is well-defined.

2.8 Beta Limit

The plasma in fusion devices is confined by a magnetic field. The strength of the toroidal magnetic field should be sufficient to stabilize the external kink mode for a given current (Hugill diagram). At the same time, the poloidal magnetic field should provide the pressure balance in the fusion device. To characterize this balance, a new variable is introduced. The beta value is the ratio of the average plasma pressure and magnetic field pressure:

$$\beta = \frac{\langle p \rangle}{\langle B^2 \rangle / 2\mu_0}. \quad (2.44)$$

Based on this definition, other variants of beta can be defined. For example, poloidal beta ($\beta_{pol} = 2\mu_0 \langle p \rangle / \langle B_\theta^2 \rangle$) is defined relative to the poloidal magnetic field (B_θ). In this part we discuss two main beta limits for tokamak plasmas and their consequences for the operation space of the tokamak. The first limit arises from equilibrium force balance. In the tokamak configuration, the plasma is bent to avoid the end losses along the magnetic field, but this bending generates three forces—all directed outward along the major radius. These forces are [28]:

- The “hoop force”, which is the same as the outward expansion force for a current in a circular loop of wire. The poloidal magnetic field, produced by the plasma current, is higher at the inner side of the torus. Thus, the resulting Lorentz force is directed outward, which leads to expansion of the current ring (see Fig. 2.16a).
- The “1/R force” is associated with the 1/R decay of the toroidal magnetic field from the inner side of the torus to the outer side. The plasma is usually diamagnetic ($\beta_{pol} > 1$), producing the field inside the plasma that partially cancels the applied toroidal magnetic field. In this situation, the forces on the high field side and on the lower field side are different, which provides the net outward force. In the opposite, paramagnetic situation ($\beta_{pol} < 1$), the net force is directed inward (see Fig. 2.16b).
- The “tire tube force” has a hydraulic nature and appears due to the difference in the inner and outer torus surfaces for the same pressure in the tube (see Fig. 2.16c).

The sum of all these forces has to be balanced in the device. In the presence of a perfectly conducting wall, the outward shift of the plasma compresses the flux at the low field side of the device and the increased magnetic field provides a restoring force in the inward direction as shown in Fig. 2.16d. This restoring force is not enough to completely suppress the outward force due to resistive decay, and this is typically done by an applied vertical magnetic field. Superposition of this vertical field on the poloidal magnetic field leads to X-point formation on the high field side of the tokamak. With increase of the plasma pressure, a higher vertical field is required to balance the forces and the X-point moves in the direction of the

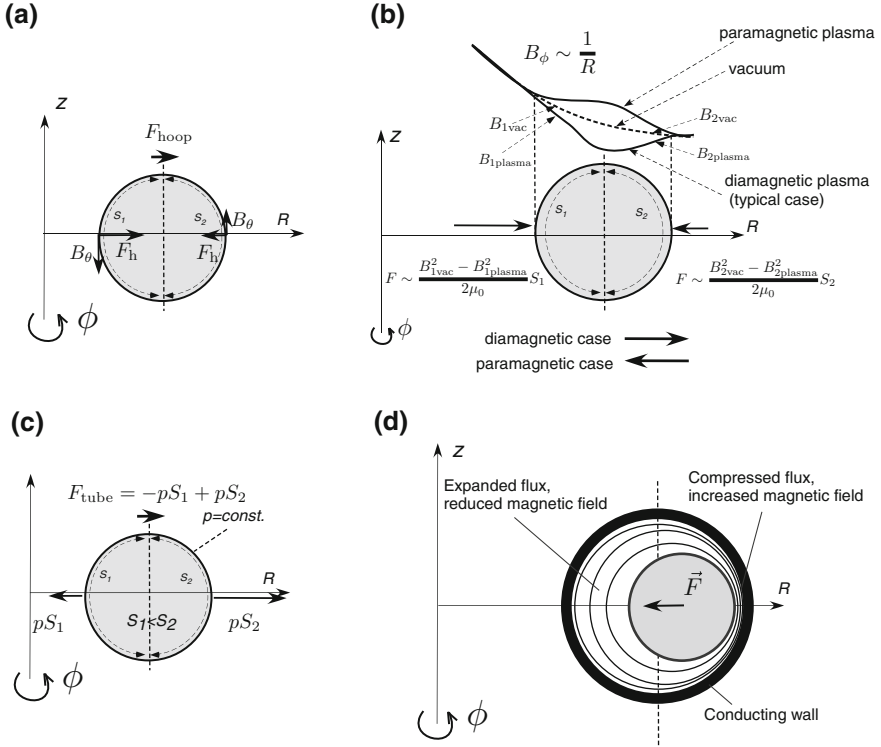


Fig. 2.16 Different forces acting on the plasma are shown schematically for a circular cross-section tokamak. **a** The “hoop force” is the same as the outward expansion force for a current in a circular loop of wire. Assuming only the surface current for a torus, one gets variation of the result poloidal magnetic field from the plasma current, I_p . This poloidal magnetic field is higher at the inner side of the torus and the result magnetic force has outward direction. **b** The “1/R force” is associated with the decay of the toroidal magnetic field, $B_\phi \sim 1/R$, from the inner side of the torus to the outer side. One obtains the force from the difference between the vacuum and plasma magnetic field taking into account the field decay. **c** The tire tube force is due to the difference in the inner and outer torus surfaces for the same pressure in the tube. The inner surface is smaller than the outer surface, $s_1 < s_2$. **d** Outward plasma movement leads to flux compression at the *low field side*. A higher magnetic field at this point produces an inward restoring force

plasma boundary. The plasma has reached its equilibrium β limit when the X-point touches the plasma surface (Fig. 2.17). Further attempts to increase β require cutting off and eliminating the inside portion of the plasma. For a fixed geometry, the actual limit is a limit on β/I_p^2 . For tokamaks with circular cross-section this limit can be written in the following form [28]:

$$\left(\frac{2\pi a^2 B_0}{\mu_0 R_0 I_p} \right)^2 \frac{\beta}{\varepsilon} \leq \frac{\pi}{16} \approx 0.62 \quad (2.45)$$

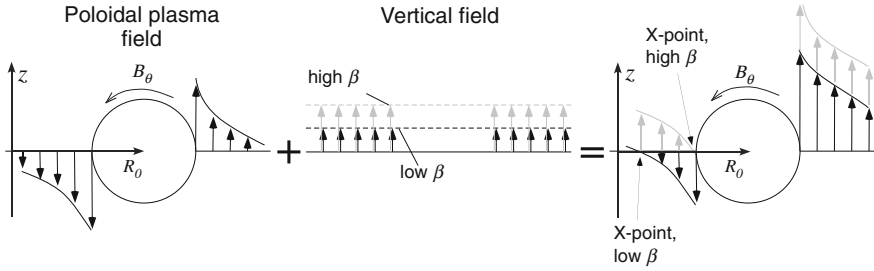


Fig. 2.17 Combination of the poloidal magnetic field (from plasma current) and external vertical magnetic field forms X-point at the *high field side* (inner side of the torus). With increase of the plasma pressure, a higher vertical field is required to balance the forces and the X-point moves in the direction of the plasma boundary. The plasma has reached its equilibrium β limit when the X-point touches the plasma surface

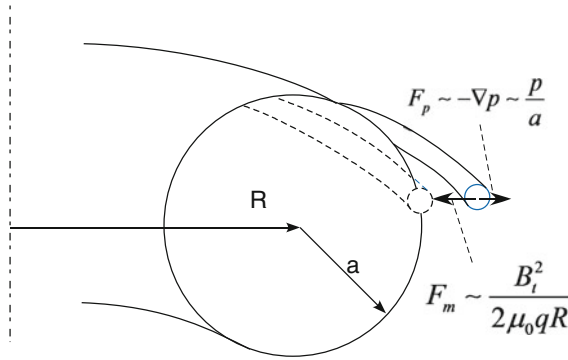


Fig. 2.18 A flux tube with length $L \sim qR$ is shifted outwards by plasma pressure. The situation is stable only if the magnetic force is sufficient to counteract the pressure force

The second β limit is connected to the final achievable pressure with respect to ballooning modes. These modes result from the toroidal geometry of the tokamak magnetic field, which implies a stronger field at the inner part of the torus ($B_\phi \sim 1/R$, where R is the major radius). Thus, the outer side of the torus has a lower magnetic field and is more sensitive to the perturbations. The physical nature of the ballooning beta limit comes from the energy balance for a particular flux tube exploring the destabilizing unfavorable curvature on the low field side (Fig. 2.18). This is shown schematically in the Fig. 2.18.

In tokamak geometry, the length of the flux tube at the low field side is proportional to the major radius and safety factor: $L \sim qR$ [1]. The stabilizing energy contribution comes from the magnetic tension force (2.22). This force can be estimated as follows:

$$F_m = \frac{(\vec{B} \cdot \nabla) \vec{B}}{\mu_0} \sim \frac{B_\phi^2}{L} = \frac{B_\phi^2}{qR}, \quad (2.46)$$

and the corresponding change in energy due to the displacement of the flux tube ξ is

$$\delta W_m = \int \vec{F}_m \cdot \vec{\xi} dV \sim \frac{B_\phi^2}{qR} \xi. \quad (2.47)$$

This energy should be sufficient to compensate the destabilizing pressure contribution. The pressure force is approximately

$$F_p \sim -\nabla p \sim \frac{p}{a}, \quad (2.48)$$

where a is the minor radius.

$$\delta W_p = \int \vec{F}_p \cdot \vec{\xi} dV \sim \frac{p}{a} \xi \quad (2.49)$$

$$\delta W_m \sim \delta W_p \rightarrow \frac{B_\phi^2}{qR} \sim \frac{p}{a} \quad (2.50)$$

Taking into account the definitions of the edge safety factor (2.39) and beta (2.44) one obtains the dependence of the maximum beta on the plasma current, magnetic field and minor radius:

$$\beta_{crit} \sim \frac{I_p}{B_\phi a}. \quad (2.51)$$

Historically, this relation was first formulated by Troyon based on ideal MHD stability simulations [29]. In these simulations Troyon and co-authors investigated the stability of the plasma with respect to all ideal instabilities: external kink modes, ballooning-kink modes, internal kink modes, etc. It was shown that the typical limit is set by kink modes with the same dependence as above:

$$\beta_{crit} = \beta_N \frac{I_p}{B_\phi a}, \quad (2.52)$$

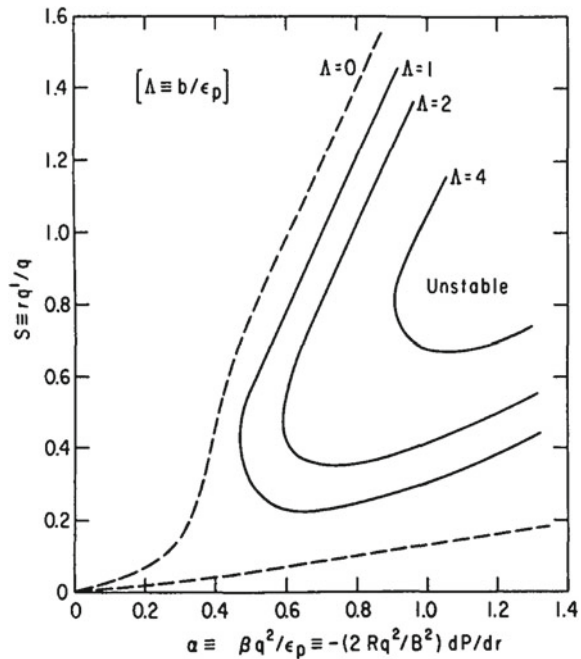
where β_N varies depending on the plasma profile, plasma shape and other factors. This value is typically around 3×10^{-2} but in the fusion community it is typical to write this value as a percentage, omitting the percent indices (in our case this will be $\beta_N = 3$ instead of 3 % or 3×10^{-2}). The maximum beta defined by Troyon includes only the plasma part. An external conducting structure can stabilize instabilities and lead to other normalized values of beta. This will be discussed in

details in the Resistive Wall Mode Chap. 6, where a normalized beta will be defined for two situations (with and without ideal wall) for the same plasma.

Numerical investigation of the ballooning stability reveals that there are two stability regions for plasma operations [30]. It is expected that at low radial pressure gradient values the pressure-driven ideal ballooning modes are stabilized by field line bending. This leads to the first stability window at low pressure gradient ($\alpha = -\frac{2\mu_0 R q^2}{B^2} \frac{dp}{dr}$) and large shear value ($s = \frac{r}{q} \frac{dq}{dr}$). The local value of the magnetic shear s shows how strong are the changes in helicity between neighboring flux surfaces. It is also a characteristic of the current profile gradient, because the safety factor is inversely proportional to the integrated current inside the flux surface. High shear is in general favorable for the plasma stability. The more surprising result is the existence of a second stability region at low magnetic shear and high pressure gradient. This is connected to the local stability of the ballooning modes in the negative shear case, which corresponds to a flat or reversed q -profile. Increase of the pressure in the tokamak builds up the pressure gradient and increases the Shafranov shift. These two modifications of the equilibrium extend the negative local shear into the favorable curvature region, which provide global stability in the second region [31].

The first and second stability regions are typically separated in the ideal MHD approximation (Fig. 2.19, dashed curves). The plasma shape, current profile and pressure profile determine the boundary of the stable regions in ideal MHD. The situation in a real plasma is more complex and effects beyond the fluid

Fig. 2.19 Stability boundaries for ballooning modes as a function of the shear parameter and the pressure parameter at various values of finite gyroradius parameter $\Lambda = b/\epsilon_p$ (The figure is from [32]. © IAEA. All rights reserved.)



approximation have to be taken into account. For example, finite Larmor radius, r_L , effects influence plasma stability and provide stronger stabilization for higher values of the finite gyroradius parameter $\Lambda = b/\varepsilon_p$, where $b \equiv \frac{n^2 q^2 r_L^2}{r^2 2}$ is a measure of the stabilizing gyroradius contributions and $\frac{1}{\varepsilon_p} \equiv -R \frac{d(\ln p)}{dr}$ is a measure of the destabilizing pressure-driven forces [32].

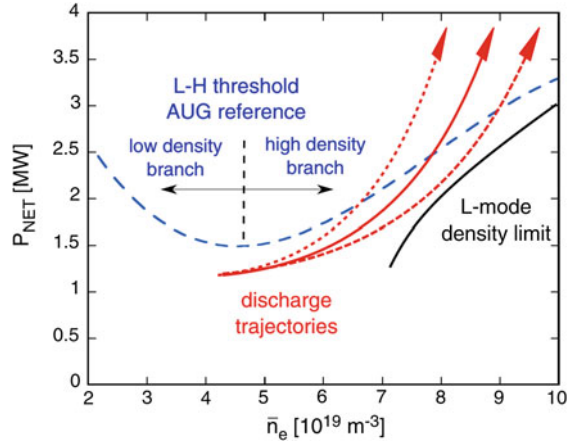
In stellarators, the plasma behavior at the beta limit is similar to its behavior at the density limit. There are no disruptive events and the beta limit manifests itself as a soft limit. Moreover, the archived values of beta clearly exceed the predicted linear stability boundaries for pressure-driven MHD modes [33]. Global MHD modes, which were found in stellarators, are consistent with predictions based on the linear stability theory. However, in most cases the observed modes saturate on a harmless level, which allows further increase of beta. Therefore, the linear stability threshold significantly underestimates the achievable beta [34]. The highest values archived in stellarators are $\langle \beta \rangle \approx 3.4\%$ (W7AS, Germany) and $\langle \beta \rangle \approx 5\%$ (LHD, Japan) [35].

2.9 Different Plasma Scenarios and their Limits

A remarkable finding in fusion plasmas is the existence of different confinement regimes: low confinement mode (L-mode), high confinement mode (H-mode) and advanced operation regime with internal transport barrier (ITB). It was first found at the ASDEX tokamak [36], that under certain conditions there is an abrupt transition to higher confinement values. Normally, auxiliary heating of the plasma enhances the radial transport perpendicular to the magnetic field lines (L-mode), but a combination of increased heating power and a divertor configuration leads to the formation of a barrier region with reduced transport at the plasma edge (H-mode). The dominant role in the transition is played by the shear of the radial electric field, E_r , which appears during L-H transition. The threshold of the transition to H-mode is independent of the type of heating as seen in Fig. 2.20 [37]. The H-mode has been reliably observed in many tokamaks of different sizes, aspect ratios, plasma currents and magnetic fields. The extrapolation from different tokamaks for the H-mode regime leads to a scaling of confinement time for the so-called “standard” H-mode. This scaling has been used as basis for the ITER design. At the same time, the physics of the barrier formation is not well understood. The dominant idea is that at high power levels strongly sheared flow velocities develop near the plasma edge that act to stabilize micro-turbulence. The L-H transition, as well as other transport barriers, remains an area of active research.

The advanced tokamak scenario aims to extend the H-mode regime to higher plasma performance in the presence of the internal transport barrier at the middle of the plasma radius. The “standard” H-mode operation does not allow conditions to be reached where the plasma is completely non-inductively driven, which limits the duration of the plasma discharge in a tokamak. The advanced scenario

Fig. 2.20 Plasma density and heating power must be increased simultaneously, remaining above density limit, for transition into H-mode (The figure is from [37]. © IAEA. All rights reserved.)

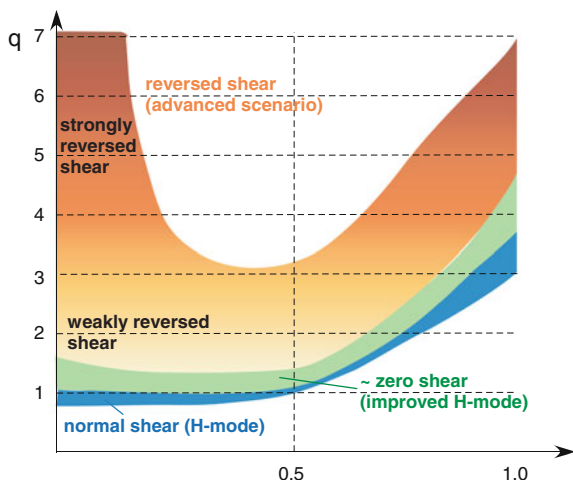


promises to achieve the steady state operation substituting the inductively driven current by bootstrap current [3]. This scenario is more disruptive and not as robust as the H-mode.

The current density profile, and hence the safety factor profile, plays an important role in plasma stability and confinement. The slope of the current profile is characterized by the magnetic shear $s = (r/q)dq/dr$ (where r is the minor radius), which is widely used in stability analysis. The “standard” H-mode profile has a safety factor value at the center, q_0 , just below 1, while at the plasma boundary, q_{95} , is 3 or higher, and the shear is always positive. The situation is completely different in the advanced scenario. It uses a range of non-monotonic q -profiles as shown in Fig. 2.21. Depending on the bootstrap current fraction, q_0 varies from 2 to ∞ . The later situation appears in the so-called “current hole” variants [38], when the plasma current density is zero at the magnetic axis. Tailoring and control of the current density profile is clearly the key for the development of these scenarios. It is possible to imagine a continuum of regimes between the non-inductive and inductive scenarios in which the bootstrap current is only a fraction of the total current. This situation is typical for improved H-mode’ discharges, which are characterized by a broad region in the plasma core of \sim zero shear and $q_0 \geq 1$ [39]. This scenario is also often called a “hybrid” scenario. It opens the way to either longer plasma pulse duration at reduced plasma current, or to improved performance at full plasma current. Hybrid scenarios typically require moderate additional heating during the plasma current ramp-up to allow the formation of a low central shear profile. The “improved” H-mode is a promising operation option for ITER which combines the current advantages of the standard H-mode, as well as the advanced scenario.

The basic equilibrium limits for plasma confinement have been discussed in the previous sections. MHD limitations are stricter. The ideal kink instability limits the maximum plasma current, ballooning and kink modes limit maximum achievable β_N values, etc. These are limits for the economic operation of future

Fig. 2.21 Schematic representation of different safety factor profiles corresponding to different confinement modes (The figure is inspired by similar representation by A.C.C. Sips.)



fusion power plants. However, the other instabilities set the limits well below the ideal limits in real plasmas. In the following we briefly discuss the main limiting instabilities for different plasma scenarios. All these instabilities have to be either avoided or controlled for successful operation of future fusion reactor. A special chapter is dedicated for each of them in this book. Here, we only briefly describe where the instability becomes important.

The safety factor profile of the conventional tokamak scenario contains the $q = 1$ resonant surface. The *sawtooth* oscillations, discussed in Chap. 4, develop at this resonant surface. They are associated with abrupt changes in central plasma confinement due to the growth of an $(m, n) = (1, 1)$ mode, where m and n are poloidal and toroidal mode numbers. Whilst the plasma usually survives the drop in the core temperature and density due to this instability, the triggering of other, more dangerous instabilities is the main concern. It is often observed that larger sawtooth crashes trigger a resistive instability: the *neoclassical tearing mode* (NTM). The maximum achievable beta limit in conventional scenarios is usually set by this mode (see Chap. 8). Thus, both instabilities have to be studied and controlled.

The safety factor profile in the advanced tokamak scenario is more elevated with respect to the conventional scenario. This allows to avoid sawteeth ($(1, 1) \rightarrow q = 1$) and NTM ($(3, 2) \rightarrow q = 1.5$). For even higher central safety factor values, the most dangerous $q = 2$ resonant surface of the $(2, 1)$ NTM can also be avoided. This is a positive consequence of the elevated safety factor profile. Advanced tokamak requires high bootstrap current fraction, which can only be achieved with high pressure gradients. These gradients drive the external kink instability. In the presence of a resistive wall, this kink instability is converted into the slower-growing *resistive wall mode* (RWM), as described in Chap. 6. This mode has to be stabilized to achieve the reactor relevant beta in this scenario. The same type of mode poses serious problems for RFP operation and has to be

stabilized. Due to its high reproducibility, RWMs in RFPs are ideal for testing different mode control algorithms as will be discussed later.

There are also several important issues which appear in both types of scenarios. The transition from L-mode to H-mode creates high pressure and current gradients at the plasma boundary. These gradients drive the so-called *edge localized modes* (ELMs). ELMs lead to a fast loss of energy and particles from the plasma edge. These particle and energy losses provide a high heat flux at the divertor. In particular, the peak values are crucial for the internal components. This instability has to be mitigated or suppressed to reduce the peak flux and is the subject of the Chap. 5.

Future burning plasmas will contain fast particles resulting from fusion reaction. Satisfactory confinement of the energetic fusion products for sufficiently long time that the fuel ions are heated by them to a level where they start to fuse and a self-sustained burn process is critical for future reactor. Interaction of these fast particles with MHD instabilities may destroy this heating mechanism. The main interaction is expected with Alfvénic types of modes, characterized by high mode frequency, which could effectively interact with the fast particles. This is the subject of Chap. 9 which is dedicated to *fast particle instabilities*.

Plasma confinement in a tokamak can be lost in a fast catastrophic event called *disruption*. This event produces large power and force loads on the structures that surround the plasma. In a reactor, these loads have the potential to produce unacceptable damage to the machine itself. Disruptions must be avoided or done in controllable manner (to avoid severe damage). Also, there can be different reasons for disruptions, and all related points are discussed in a special disruption Chap. 7 of this book.

Important instabilities in the stellarator concept differ compared to the tokamak. Some instabilities either do not exist (current driven modes) or are much less dangerous (pressure driven modes). At the same time, the fast particle modes (Chap. 9) are probably more important for stellarators. The 3D nature of magnetic field produces an even larger number of potentially unstable modes in stellarators, compared to 2D tokamaks. Fast particle confinement is the subject of current research and is one of the key points to investigate in ITER.

2.10 Further Reading

Overview of the operation space in this chapter is an attempt to provide concise description of the main operation limits. It is not possible to discuss all details within this format. There are several books which nicely cover first part of this chapter and can be recommended for further reading.

- J.P. Freidberg, “Plasma Physics and Control Fusion”, Cambridge University Press, 2007 (This book gives nice description of main concepts of magnetic fusion).
- More advanced description can be found in “Fusion Physics”, Ed. M. Kikuchi et.al., IAEA VIENNA, 2012, (this book is freely available online <http://www-pub.iaea.org/books/iaeabooks/8879/Fusion-Physics>).

- Tokamaks are discussed in the famous book of J. Wesson, “Tokamaks”, 4th Edition, Clarendon Press, Oxford, 2011.

There are several books which discuss magneto-hydrodynamic theory and MHD instabilities with different level of required background:

- J.P. Freidberg, “Ideal Magnetohydrodynamics”, Plenum Press, New York and London, 1987 (This is one of the best standard textbooks for MHD).
- Hartmut Zohm “Magnetohydrodynamic Stability of Tokamaks”, Wiley-VCH, Weinheim, Germany, 2014 (The book gives nice description of the MHD instabilities and their connection to the operation limits in tokamak).
- D.D. Schnack, Lectures in Magnetohydrodynamics: With an Appendix on Extended MHD, Lect. Notes Phys. 780 (Springer, Berlin Heidelberg 2009) (This book provides detail derivation of main MHD concepts and will be extremely useful for students).
- J.A. Bittencourt, “Fundamentals of Plasma Physics”, 3ed Edition, Springer 2004 (Connection of the kinetic and the fluid descriptions is nicely shown in this book).
- Johan Peter Goedbloed and Stefaan Poedts, “Principles of Magnetohydrodynamics: With Applications to Laboratory and Astrophysical Plasmas”, Cambridge University Press, 2004 and J.P. Goedbloed, Rony Keppens, Stefaan Poedts, “Advanced Magnetohydrodynamics: With Applications to Laboratory and Astrophysical Plasmas”, Cambridge University Press, 2010 (These two volumes give extremely detailed description of MHD theory starting from basic assumptions).
- A B Mikhailovskii, “Instabilities in a Confined Plasma”, IOP Publishing, 1998, (This book is focused on MHD experts and discusses systematically theory of MHD instabilities).

Different aspects of the operation limits in tokamaks are described in the following books and papers:

- L. C. Woods, “Theory of Tokamak Transport. New Aspects for Nuclear Fusion Reactor Design”, Wiley-VHC Verlag GmbH Weinheim, 2006 (Some aspects of the MHD and thermal limits can be found in this book).
- R. Koslowski, “Operation Limits and Limiting Instabilities in Tokamak Machines”, Transaction of Fusion Science and Technology, Feb. 2006, Vol 49, p. 147. (The paper gives nice and very concise introduction into the subject).
- D. Frigione, “High-density operation in tokamaks”, Rivista del Nuovo Cimento Vol. 22, N8, 1999, p. 1 (Mainly density and radiation limits are discussed).
- M Greenwald, “Density limits in toroidal plasmas”, Plasma Phys. Control. Fusion 44 (2002) R27–R80 (This is a detailed review of the density limit).

References

1. J. Wesson, “*Tokamaks*”, 3rd edn. (Clarendon Press Oxford, Oxford, 2004)
2. N.J. Fisch, *Rev. Mod. Phys.* **59**, 59175 (1987)
3. A.G. Peeters, *Plasma Phys. Control. Fusion* **42**, B231 (2000)
4. M. Shimada et al., *Nucl. Fusion* **47**, S1 (2007)
5. E.M. Kikuchi et al., *Fusion Physics*, IAEA (2012), <http://www-pub.iaea.org/books/IAEABooks/8879/Fusion-Physics>
6. J.A. Bittencourt, *Fundamentals of Plasma Physics*, 3rd edn. (Springer, Berlin, 2004)
7. D. Biscamp, *Nonlinear MHD* (Cambridge University Press, Cambridge, 1993)
8. J. Freiberger, *Ideal MHD* (Plenum Press, New York, 1987)
9. P. Goedbloed, *Advanced Magneto-Hydrodynamics* (Cambridge University Press, Cambridge, 2010)
10. L. Harra, K. Mason (eds.), *Space Physics* (Imperial College Press, London, 2004)
11. D.D. Schnack, *Lectures in Magnetohydrodynamics: With an Appendix on Extended MHD*, Lecture Notes Physics (Springer, Berlin, 2009), p. 780
12. A.B. Mikhailovskii, *Instabilities in a Confined Plasmas* (IOP Publishing, Bristol, 1998)
13. J. Wesson, *Nucl. Fusion* **18**, 1 (1978)
14. H.J. de Blank, *Trans. Fusion Sci. Technol.* **49**, 111–118 (2006)
15. D. Frigione, *Rivista del Nuovo Cimento* **22**, 1 (1999)
16. M. Greenwald, *Plasma Phys. Control. Fusion* **44**, R27–R80 (2002)
17. M. Greenwald, *Nucl. Fusion* **28**, 2199 (1988)
18. W.M. Stacey, *Fusion Sci. Technol.* **52**, 29 (2007)
19. W. Suttrop et al., *Plasma Phys. Control. Fusion* **39**, 2051 (1997)
20. J. Rapp et al., Scaling of density limits with respect to global and edge parameters in TEXTOR-94, in *Proceedings of 26th International Conference on Control Fusion and Plasma Physics*, Maastricht, vol. 23. European Physical Society, Geneva (1999), p. 665
21. P.T. Lang, *Nucl. Fusion* **52**, 023017 (2012)
22. D.A. Gates et al., *Phys. Rev. Lett.* **108**, 165004 (2012)
23. S. Sudo, *Nucl. Fusion* **30**, 11 (1990)
24. R. Gruber et al., *Comput. Phys. Commun.* **21**, 323 (1981)
25. L.C. Bernard et al., *Comp. Phys. Commun.* **24**, 377 (1981)
26. W. Kerner et al., *J. Comput. Phys.* **142**, 271 (1998)
27. F. Hofmann et al., *Nucl. Fusion* **40**, 767 (2000)
28. J. Freiberger, *Plasma Physics and Fusion Energy* (Cambridge University Press, Cambridge, 2007)
29. F. Troyon et al., *Plasma Phys. Control. Fusion* **26**, 209 (1984)
30. A. Sykes et al., *Plasma Phys. Control. Fusion* **29**, 719 (1987)
31. K. Miyamoto, *Plasma Physics and Controlled Nuclear Fusion* (Springer, Berlin, 2005)
32. W.M. Tang et al., *Nucl. Fusion* **21**, 891 (1981)
33. K.Y. Watanabe et al., *Nucl. Fusion* **45**, 1247–1254 (2005)
34. A. Weller et al., *Fusion Sci. Technol.* **50**, 158 (2006)
35. A. Komori et al., *Nucl. Fusion* **49**, 104015 (2009)
36. F. Wagner et al., *Phys. Rev. Lett.* **49**, 1408 (1982)
37. F. Rytter et al., *Nucl. Fusion* **52**, 114014 (2012)
38. T. Fujita, *Nucl. Fusion* **50**, 113001 (2010)
39. J. Stober et al., *Nucl. Fusion* **47**, 728 (2007)
40. D. Meade, *Nucl. Fusion* **50**, 014004 (2010)

Active Control of Magneto-hydrodynamic Instabilities in
Hot Plasmas

Igochine, V. (Ed.)

2015, XV, 342 p. 153 illus., 86 illus. in color., Hardcover

ISBN: 978-3-662-44221-0